

Arctic regional changes revealed by clustering of sea-ice observations

Amélie Simon^{1,2}, Pierre Tandeo^{1,3}, Florian Sévellec^{2,3},
Camille Lique²

¹ IMT Atlantique, Lab-STICC, UMR CNRS 6285, 29238, Brest, France

² Univ Brest CNRS Ifremer IRD, Laboratoire d'Océanographie Physique et Spatiale (LOPS), Brest, France

³ ODYSSEY Team-Project, INRIA CNRS, Brest, France

Correspondence: Amélie Simon (amelie.simon@ifremer.fr)

35 Abstract

36 Understanding the evolution of Arctic sea-ice is crucial due to its climatic and
37 socio-economic impacts. Usual descriptors (e.g., sea-ice extent, Marginal Ice Zone,
38 sea-ice age, and ice-free duration) quantify changes but do not account for the full
39 seasonal cycle. Here, using satellite observations of sea-ice concentration (SIC) over
40 1979-2023, we perform a k-means clustering of the Arctic sea-ice seasonal cycle,
41 initializing with equal quantile separation and using Mahalanobis distance. Without
42 providing prior information, this data-driven method shows that the Arctic is best
43 described by four types of seasonal cycles: open-ocean (no ice year-round), permanent
44 sea-ice (full coverage with a minimum of 70% SIC), and two clusters showing ice-free
45 conditions ($SIC < 0.15$), namely partial and full winter freezing. The latter has larger
46 SIC in winter, more abrupt melting and freezing periods, and a shorter ice-free season
47 than the former. This reduction of dimension in the data suggests that the first date of
48 retreat is a good indicator for ice-free conditions the following summer and the first
49 date of advance a good indicator for fully ice cover conditions the following winter. We
50 introduce the probability to belong to each four seasonal cycles as a descriptor to
51 monitor Arctic sea-ice changes. The pan-Arctic probability to belong to the permanent
52 sea-ice seasonal cycle has decreased by 3.1 %/decade which is compensated with an
53 increase of probability to belong to the open-ocean cluster (1.6 % per decade), the full
54 winter freezing cluster (1.1 % per decade) and the partial winter-freezing cluster (0.5 %
55 per decade). Regionally, the permanent sea-ice retraction from the Pacific side is
56 compensated by the full winter-freezing cluster while the open-ocean cluster
57 expansion in the Atlantic side is lost by the partial winter-freezing cluster. The new
58 classes of partial and full winter freezing are helpful for sea ice process understanding
59 as it refines the classical MIZ category into two distinct sea-ice clusters. The trend is
60 primarily controlled by the tendency of the more abrupt melting and growth seasonal
61 cycle (full winter-freezing cluster) compared to the trend of the quasi-sinusoidal
62 sea-ice seasonal cycle (partial winter-freezing cluster). Also, from the Beaufort to the
63 Kara Seas, the southern parts have stabilized (experiencing a new typical seasonal
64 cycle, corresponding to the full winter-freezing cluster) and the northern part have
65 destabilized (losing their typical permanent sea-ice seasonal cycle). Therefore, this

66 work provides a new way to describe Arctic regional changes using a statistical
67 framework based on physical behaviours of sea-ice. Our study calls for a more
68 latitudinal vision of the Arctic regions.

69

70 Short summary

71 Through a machine learning technique based on seasonal cycles of sea-ice
72 concentration from satellite data over the last four decades, our research shows that
73 four regions are sufficient to best regionalize the Arctic. These regions are mainly
74 organized into latitudinal bands and evolve in time and space. The descriptor proposed
75 to monitor Arctic sea-ice changes is the probability to belong to each region. The
76 probability to belong to the permanent sea-ice regions has decreased by 3.1 % /decade.

77

78 Keywords

79 Arctic sea-ice, seasonal cycle, machine learning, clustering, climate change, satellite
80 dataset, regionalization

81

82

83 Introduction

84 The Arctic region has experienced rapid changes over recent decades that are
85 expected to intensify in the future (Shu et al., 2022). For a global warming of 1°C, the
86 Arctic has warmed by about 2.5 °C. In a 4°C warmer world, the Arctic is projected to be
87 from 7°C to 10°C warmer (IPCC, 2021; their Figure SPM.5). One of the main
88 mechanisms behind this Arctic amplification is the retreat of sea-ice, giving way to an
89 open-ocean that captures more solar radiation, an effect called surface albedo
90 feedback (Pithan and Mauritsen, 2014; Goosse et al., 2018). The observed Arctic
91 sea-ice loss has been attributed to human influence primarily because of greenhouse
92 gas emissions dominated by carbon dioxide and methane (Eyring et al., 2021 in IPCC,
93 their section 3.4.1.1).

94 The decline of the Arctic sea-ice has profound implications for the regional
95 environment and for almost four million people living beyond the Arctic circle.
96 Reduced ice cover increases light availability, which can enhance phytoplankton
97 blooms (Vancoppenolle et al., 2013). This, in turn, reshapes the food web structure
98 (Ardyna and Arrigo, 2020) and has significant consequences for fisheries, potentially
99 impacting catch levels and spatial distribution (Stock et al., 2017). The formation and
100 melting of sea ice also largely influences nearly all aspects of life for marine mammals
101 in the Arctic. A delay in winter sea-ice formation can trigger marine mammals' unusual
102 mortality events, as it has been the case in 2018 in the Bering Sea (Siddon et al., 2020).
103 Indigenous hunting opportunities that are dependent on the presence of sea-ice have
104 decreased and shifted in time (Huntington et al., 2017). Besides, new ice-free regions
105 could open industrial shipping routes and offshore oil and gas exploration with
106 associated risks of oil spills, marine mammal strikes and noise pollution and lead to
107 tension between nations (Galley et al., 2013; Huntington et al., 2020).

108 The sea-ice retreat not only affects the Arctic locally but also plays a pivotal role
109 in the global Earth's radiative budget (Forster et al., 2021 in IPCC, their section 7.4.2.3)
110 and a potential role in the modulation of remote large-scale oceanic and atmospheric
111 circulation, known as Arctic teleconnections (Deser et al., 2015; Cohen et al., 2020;
112 Simon et al., 2021; Chripko et al., 2021; Smith et al., 2022; Cvijanovic et al., 2025).
113 Therefore, describing the evolution of the Arctic sea ice on a dynamic basis is
114 important due to its fast evolution, which has implications for both local and global
115 climate and socio-economic systems.

116 Different methods have been classically used in the literature to describe the
117 recent changes in Arctic sea-ice. Most of them are based on the analysis of sea-ice
118 concentration (SIC), which is obtained from satellite measurements since 1979 over
119 the full Arctic region. In comparison, observational datasets of sea-ice thickness are
120 available only for less than two decades and are still associated with large
121 uncertainties (Ricker et al. 2017). The sea-ice area (SIA; integral sum of the product of
122 SIC and area of all grid cells) or the sea-ice extent (SIE; integral sum of the areas of all
123 grid cells with at least 15% ice concentration) enable to highlight years with
124 exceptionally low September sea-ice cover, such as 2012 and to a smaller extent 2007,

125 2016 and 2020 (Parkinson and Comiso, 2013; Petty et al., 2018; Gulev et al., 2021 in
126 IPCC, their Figure 2.20; Bushuk et al., 2024) or quantify long-term trends. For instance,
127 the September SIE exhibits a decreasing trend of -12.7 ± 2.0 % per decade over the
128 period 1979 to 2020 (Meier and Stroeve, 2022). However, trends of SIA or SIE only
129 inform about changes in regime from ice to open-ocean and do not consider changes in
130 sea-ice features.

131 Other diagnostics have been proposed to document changes in sea-ice features.
132 A classification using thresholds of 0.15 and 0.8 SIC is commonly used and these
133 regions refer to the Marginal Ice Zone (MIZ). Rolph et al., (2020) noted that the MIZ
134 shifted northward and its extent remained relatively constant. Song et al., (2025)
135 quantify this northward shift of the MIZ of approximately $0.051^\circ/\text{yr}$. They also provide
136 insights into the evolution of the MIZ regions using two morphological parameters
137 (shape and compactness indices). They show that in late summer, MIZ evolves to a
138 smoother and more compact ice edge. The thresholds are convenient to represent a
139 category with loose and packed ice but somehow arbitrary and other definitions of the
140 MIZ have been proposed in the literature based on dynamical considerations (e.g.
141 Sutherland and Dumont 2018). Here, we quantify directly the regions without
142 arbitrary threshold nor intermediate integrated metrics.

143 Also, the age of sea-ice categorizes sea-ice into three types: open-water,
144 first-year ice and multi-year ice (Kwok et al., 2007; Regan et al., 2022). Maslanik et al.
145 (2011) show a strong decrease in the proportion of multiyear ice in the Arctic Ocean
146 during the 1980-2011 period, especially in the Canadian sector. Another diagnostic
147 deals with the duration of the ice-free period, and quantifies the timing of the
148 transition between the freezing and melting seasons. The recent Arctic sea-ice
149 reduction has resulted in a longer ice-free season (~ 5 -10 days per decade), due to both
150 earlier ice retreat and later ice advance (Stammerjohn et al., 2012; Stroeve et al., 2014;
151 Lebrun et al., 2019), especially in the Chukchi, East Greenland and northeast Barents
152 seas (Markus et al., 2009; Parkinson, 2014; Johnson & Eicken, 2016). However, these
153 diagnostics do not consider the full seasonal cycle of sea-ice, and thus do not inform on
154 the sea-ice dynamics including melting and growth behaviour.

155 These four ways of describing the variations in Arctic SIC (SIE, MIZ, sea-ice age,
156 ice-free duration), without considering directly the full sea-ice seasonal cycle, have
157 nonetheless highlighted changes in the shape of the sea-ice seasonal cycle: (i) the trend
158 in SIE (Fox-Kemper et al., 2021 in IPCC, their Figure 9.13; Meier and Stroeve, 2022),
159 the trend in MIZ fraction (MIZ extent divided by SIE; Rolph et al., 2020) and trend in
160 northward shift of the MIZ (Song et al., 2025) depends on the season, being maximum
161 in late summer (ii) Arctic sea ice has shifted to younger ice between 1979 and 2018
162 (IPCC, 2019) and (iii) the trend of later ice advance is expected to eventually double
163 that of earlier retreat over this century, shifting the ice-free season into autumn
164 (Lebrun et al., 2019). Here, in this paper, we describe the evolution of the Arctic by
165 delimiting spatio-temporal regions having a common type of seasonal cycle.

166 Regionalizations of the Arctic have been proposed previously. Parkinson et al.,
167 (1978) divided the Arctic into 8 regions based on either geographical boundaries or
168 physical criteria (e.g.; the Central Arctic encompassing the largest mass of perennial
169 sea-ice or the Greenland Sea which allows for the only deep-water connection within
170 the Arctic Basin). This regionalization was expanded by splitting regions into individual
171 seas to distinguish the behaviour of the Arctic coastal regions, resulting in considering
172 up to 15 or 18 regions (Meier et al., 2007; Peng and Meier, 2018). Besides, five climatic
173 regions of the Arctic have been defined using multiannual averages of a number of
174 meteorological elements computed for the first half of the 20th century: Atlantic,
175 Siberian, Pacific, Canadian and Baffin Bay regions (Przybylak, 2002, 2007). Other
176 regionalizations have been used to assess the influence on lower latitude climates of
177 Arctic sea-ice loss from specific areas (5 to 7 regions; Levine et al., 2021; Delhayé et al.,
178 2024). However, the criteria for the boundaries of these proposed regions are hard to
179 determine and somewhat arbitrary. A statistical regionalization method based on
180 observed SIC has been proposed for Antarctica. Raphael and Hobbs, (2014) isolates
181 regions around Antarctica by using sea ice extent decorrelation length scale and
182 variance. The resulting five sectors exhibit distinct times of sea-ice advance and
183 retreat. Their methodology does not account for the temporal evolution of the sectors.
184 The originality of our analysis resides in the fact that we regionalize the Arctic based
185 on physical criteria of the dynamics of the sea-ice seasonal cycle, therefore without

186 imposing pre-defined regions and allowing the regions to evolve in time. To do so, we
187 set up a clustering method (unsupervised machine learning).

188 Regionalizations determined from clustering methods have been shown to be
189 an efficient tool. It has been applied to ocean temperature profiles to capture coherent
190 physical changes (e.g. the water column during an El Niño event (Houghton and Wilson,
191 2020), heat distribution in the North Atlantic (Maze et al., 2017)) or on seasonal cycle
192 of phytoplankton biomass to identify bioregions in the Mediterranean (d'Ortenzio and
193 Ribera d'Alcalà, 2009). The same conceptual methodology has also been applied to the
194 polar regions. In the Antarctic, Wachter et al. (2021) described the spatio-temporal
195 sea-ice variability and documented significant spatial shifts during 1979-1998 and
196 1999-2018 by means of 10 clusters based on the seasonal cycle of sea-ice. In the
197 Arctic, Valko (2014) proposed a regionalization based on geographic and geopolitical
198 indicators, ending up with respectively two and three clusters, and Johannessen et al.
199 (2016) identified 6 major regions by clustering annual average of surface air
200 temperature. The boundaries of the defined clusters coincide with the outlines of the
201 continents and the averaged position of the sea-ice edge. Besides, clustering methods
202 for other purposes than regionalization have been used in the Arctic. Gregory et al.,
203 (2022) using a clustering analysis together with complex networks, show that climate
204 models underestimate the importance of some regions (Beaufort, East Siberian, and
205 Laptev seas) in explaining the pan-Arctic summer SIA variability. Using an ocean-sea
206 ice general circulation model, Fuckar et al. (2016) performed a k-means cluster analysis
207 on pan-Arctic detrended sea-ice thickness and found that the associated binary time
208 series of cluster occurrences exhibit predominant interannual persistence with a mean
209 timescale of about 2 years. However, no spatio-temporal regionalization based on the
210 clustering of the Arctic seasonal cycle of sea-ice has been proposed so far.

211 In this paper, we determine Arctic regions based on statistically different
212 sea-ice concentration seasonal cycles, and describe Arctic changes through the time
213 evolving borders. We identify for the first time spatio-temporal regions of the Arctic
214 based on the variability of the seasonal cycle of Arctic sea-ice concentration. We apply
215 a k-means clustering method to determine regions based on their time-evolving
216 belonging to a given type of seasonal cycle. In section 2, the dataset, domain of interest

and clustering method are detailed. In section 3, we first analyze the clustering outputs of the Arctic sea-ice seasonal cycle (3.1), then examine the probability to belong to each cluster (3.2), and finally investigate the regime stability and transition (3.3). Conclusions and discussion follow in section 4.

2. Data and Clustering Method

2.1 Sea-ice concentration (SIC)

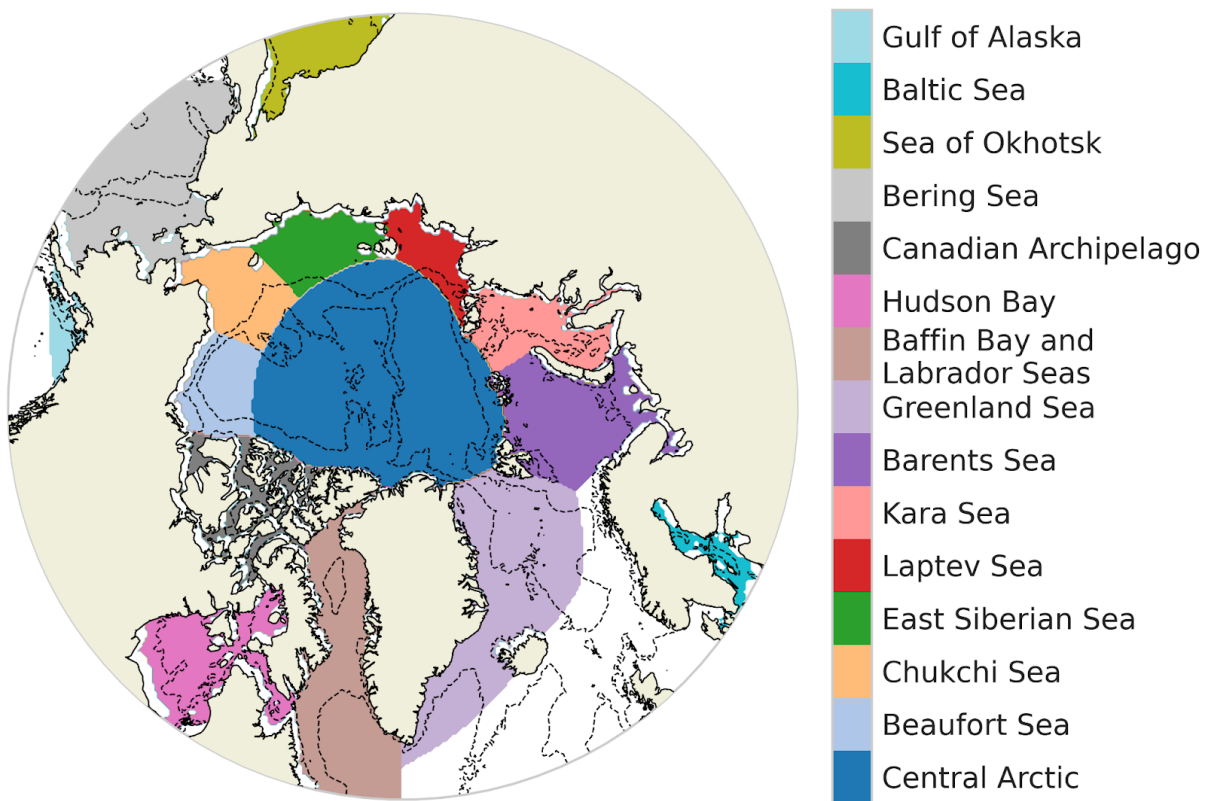
The National Snow and Ice Data Center (NSIDC) provides gridded SIC fields on a 25 km polar stereographic projection obtained from passive microwave satellite measurements on daily temporal resolutions. We use the climate data record (CDR) product (Meier et al., 2021), which is based on the most recent approach combining the NASA team (NT; Cavalieri et al., 1984) and the bootstrap (BT; Comiso et al., 1986) algorithms. Because of the tendency of passive microwave measurements to underestimate concentration, the CDR chooses the higher concentration between the NT and BT algorithms and assigns it to each grid cell. The pole hole - the region around the North Pole where satellite measurements are unavailable - is filled from the average concentration of the circle of surrounding adjacent grid cells. The size of the pole hole has diminished over time due to advancements in satellite technology. Measurement uncertainties are highest at low SIC, where satellite signals are often influenced more by atmospheric and surface conditions—such as clouds, water vapor, melt on the ice surface, and changes in the character of the snow and ice surface—than by the actual presence of ice. We utilize daily data from January 1979 to December 2023, using linear interpolation for the few missing data and compute mean values every 5 days. The 29 February of every bissextile year is removed before computing the 5-day mean. We choose this 5-day temporal resolution as similar results are found for a daily temporal resolution whereas a monthly temporal resolution shows small differences in the spatial distribution of clusters (Figure S1). Sensibility tests suggest that 45 years of data are long enough to obtain a robust signal, as close clusters are obtained using periods of 20 years, 30 years and 40 years (Figure S2). Throughout the manuscript, sea-ice will always relate to concentration.

247

248 2.2 Studied domain

249 The study considers the ocean above 55°N. The description of the domain is
250 based on the delimitation provided by NSIDC (Meier et al., 2023) and encompasses 15
251 classically predefined regions (Figure 1). The bathymetric data is derived from the
252 GEBCO 2024 Grid (GEBCO Compilation Group, 2024).

253



254

255 Figure 1: Geographical decomposition of the Arctic Ocean (defined as ocean above
256 55°N) into 15 regions following Meier et al. (2023). Bathymetry contours -100 m and
257 -2000 m are drawn with a dotted line.

258

2.3 Clustering set up

We consider all oceanic grid cells above 55°N having a non-zero sea-ice seasonal cycle (having at least a non-zero value for SIC throughout the year). Hence, the number of considered grid cells depends on the year. Grid cells with a zero sea-ice seasonal cycle are reintroduced after the clustering in order to define an open-ocean cluster. This favours a separation between regimes with and without sea-ice. The input data of our clustering are all the seasonal cycles including every considered grid cell and every year. In practice, we are thus working with a matrix with rows containing every considered grid cell of the period 1979-2023, here called points (1123710 elements) and columns containing every time step for one year, here 5-day mean (73 elements). A schematic of this matrix input data for the clustering is presented Figure 2a.

We implement a k-means clustering algorithm, which is an unsupervised machine learning method that groups data into subsamples sharing common features (Jain et al., 2010). It has the advantage of being non-parametric as our data distribution is strongly non-Gaussian. Indeed, SIC is bounded between 0 and 1 with high occurrences of values close to 0 and 1. It is an iterative method that minimizes a cost function being the sum of the squared distance (distance in a sense that would be defined later) between each seasonal cycle and its nearest cluster center (also called centroid). At each iteration, the coordinates of the centroids are updated. The initialization of centroids coordinates using k-means++ concept (the first centroid is chosen randomly, the second is the farthest-away, the third the farthest-away of the first and second, and so on) has been tested and is partly impacting our results. Therefore, we choose a different initialization strategy. We initialize the centroids coordinates based on seasonal cycles that separate the data into equal quantiles. For a clustering involving two clusters, the initializations are the two seasonal cycles of 0.33 and 0.66 quantiles of all seasonal cycles; for a clustering involving three clusters, the initializations are the three seasonal cycles of 0.25, 0.5, and 0.75 quantiles, and so on (Figure 3b). The quantiles are calculated over all the seasonal cycles considered in this study. This favours initial centroids far from each other to avoid iterating over a local minimum and the clustering is thus deterministic (i.e., it does not present any random

aspect). The strategy of initialization based on quantiles has been investigated for synthetic and real dataset and has shown a faster convergence compared to random and Kmeans++ initialization techniques (Jambudi and Gandhi, 2022).

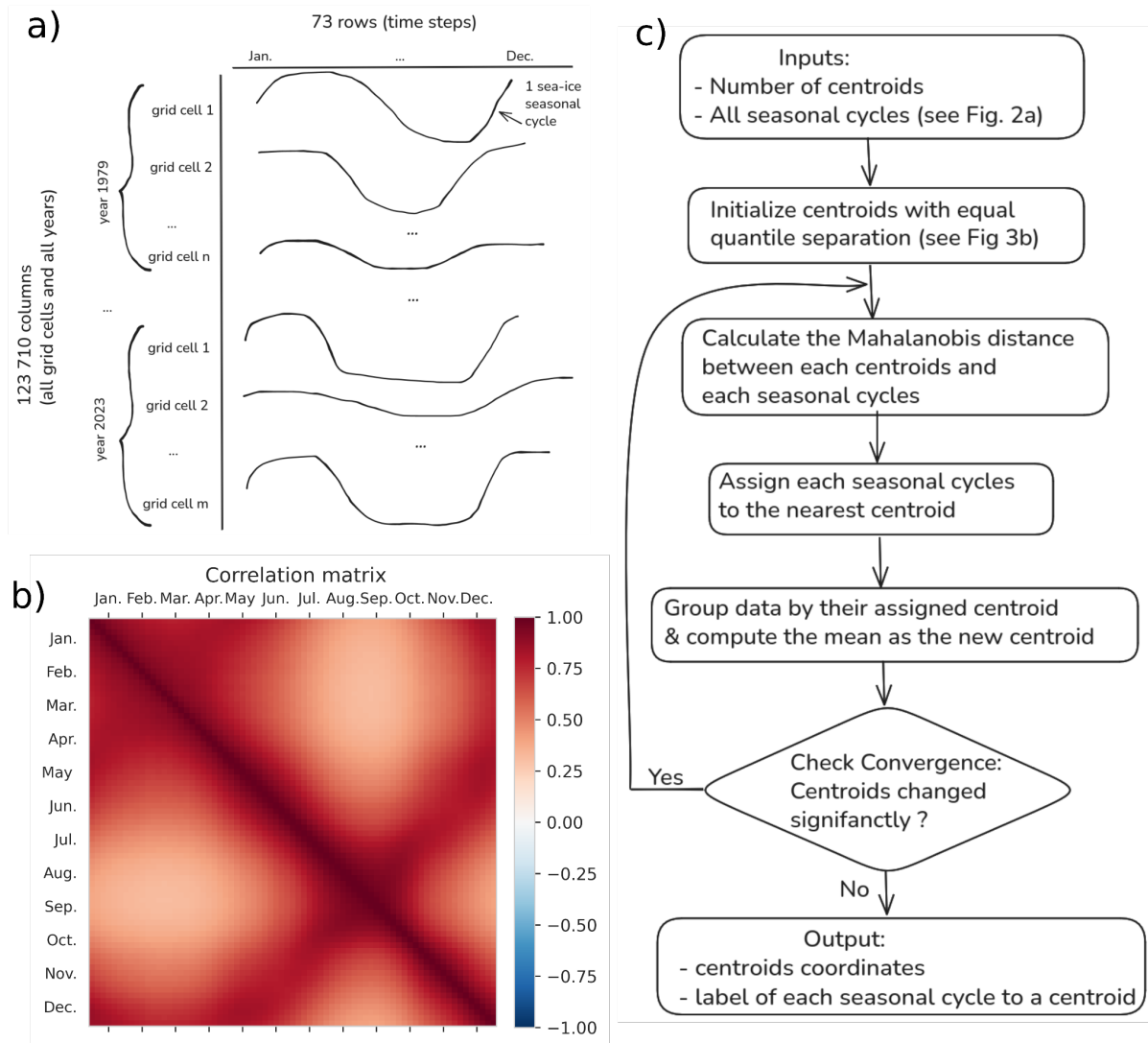


Figure 2: Schematic of the matrix input data for the k-means clustering (panel a), correlation matrix of the 5-day mean SIC for all non-zero sea-ice seasonal cycle above 55°N (panel b) and algorithm flow chart of the clustering (panel c)

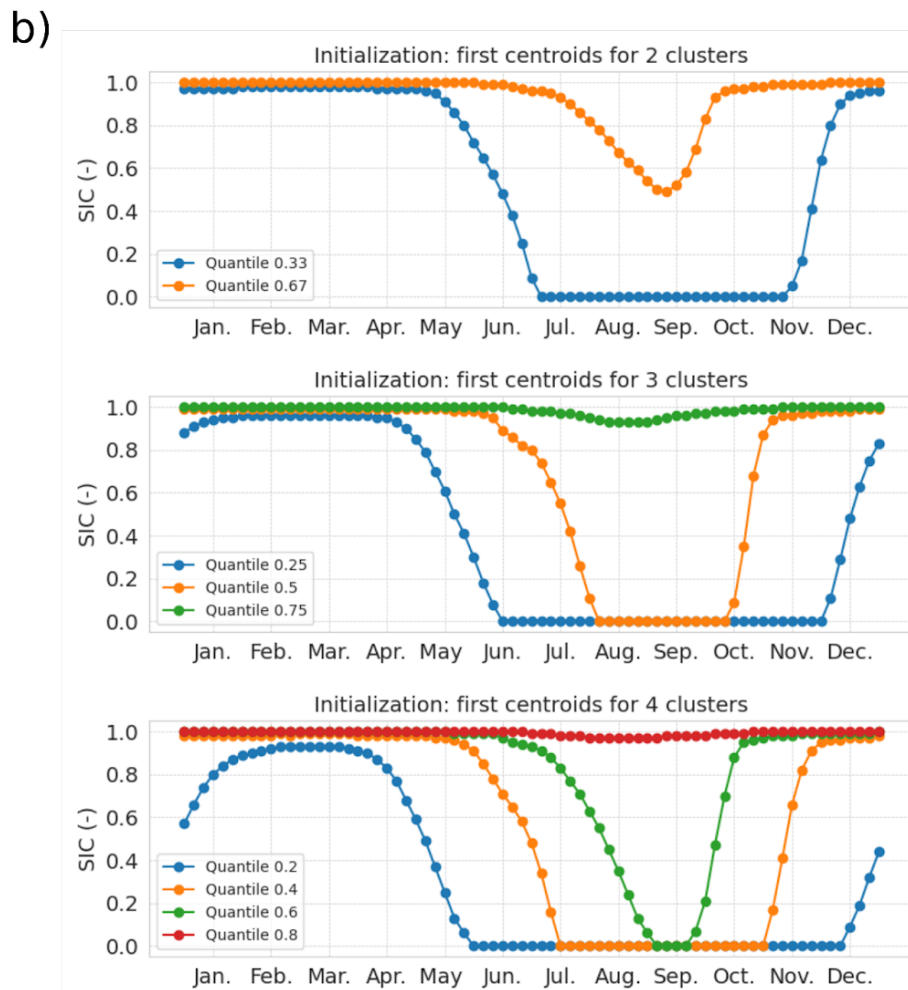
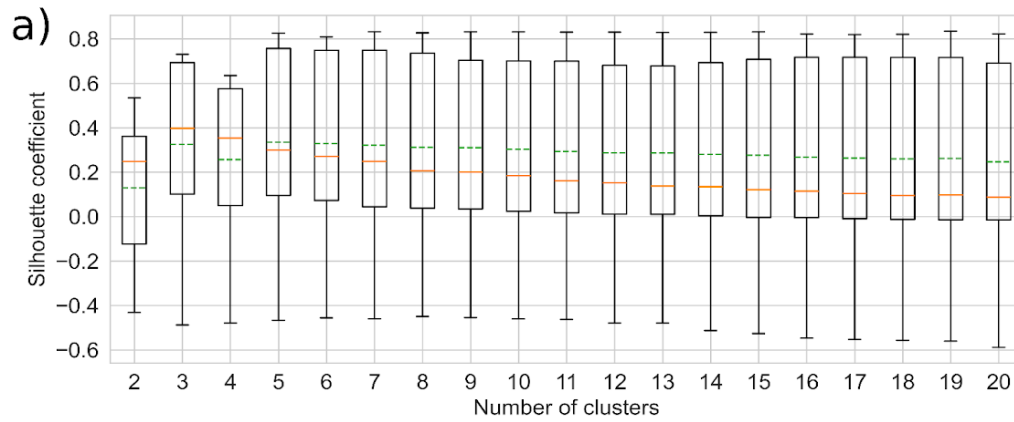
The clustering algorithm is based on the calculation of distances. The Euclidean distance is often used in similar methods, yet, here, we choose to use the Mahalanobis distance (using the correlation matrix) to constrain the clustering with physical information. All the combinations of 5-day mean SIC have a positive correlation, as shown in Figure 2b by the correlation matrix. The correlation matrix is computed for all nonzero seasonal cycles for the period 1979-2023 above 55 °N. It is calculated from

the matrix of shape (73, 1123710), having 1123710 value of SIC for 73 dates. Notably, a strong correlation exists between spring and autumn (June and November), while the weakest correlations are between summer and winter (March and September, minimum correlation is 0.31). As data are correlated, a privileged direction exists when plotting the SIC for all grid cells and all years of a given date (5-day mean) against another date. We consider this physical relation of temporal dependency by using the Mahalanobis distance (which we defined as an Euclidean scalar product normalized by the inverse of the correlation matrix) in the clustering algorithm. A 5-day mean SIC strongly correlated with another (such as spring and autumn) has a reduced distance compared with Euclidean distance. We note that, as we want to conserve the physical information of the variability intensity for each 5-day mean SIC, we do not normalize the distance by the covariance matrix (as usually done for the Mahalanobis distance) but by the correlation matrix that only takes into account relation between different 5-day mean SIC. As a result, a 5-day mean SIC with weak variability (as in winter) will have a smaller impact on the total seasonal cycle than a 5-day with larger variability (as in summer). Therefore, we do not modify the relative weight (based on the variability) of each 5-day mean SIC.

The Mahalanobis norm, deriving from a symmetric operator, effectively rotates the original physical phase space (here, date of the annual cycle) to align with the data's natural directions—linear combinations of the physical time axis. This transformation allows centroid detection in a space that reflects the intrinsic structure of the data. Therefore, using the Mahalanobis distance helps the clustering algorithm to follow the direction of the correlation and capture the elongated shapes of clusters. When calculating the probability to belong to one cluster, we do not need to work with the data's natural directions, but rather work in the original physical time space. Therefore we use Euclidean distance for the calculation of probability and the correlation-based Mahalanobis distance for the clustering. An algorithm flow chart of the clustering is displayed Figure 2c.

Clustering methods are a type of unsupervised learning technique where the number of underlying classes, called clusters, is unknown beforehand. Consequently, one must test several choices for the number of clusters, k . For each chosen value of k ,

a metric must be calculated to evaluate the resulting partition. The Silhouette coefficient is a metric classically used for this purpose (Rousseeuw, 1987; Houghton and Wilson, 2020). The general idea is to measure how similar an object is to its own cluster compared to other clusters; a high Silhouette value means the object is well matched to its own cluster and poorly matched to neighboring clusters. Indeed, the larger the Silhouette coefficient is (bounded between -1 to 1), the farther the centroids are from each other and the more grouped are the points of the same cluster. It measures the quality of the clustering when seeking for compact and well-separated clusters. Ultimately, the number of clusters that maximizes the Silhouette coefficient is the optimal choice retained for the final clustering solution. We rely on the `Silhouette_sample` function from the python package `sklearn.metrics` (Pedregosa et al., 2011), which calculates the Silhouette coefficient for every point as $(b - a) / \max(a, b)$ where a is the mean intra-cluster distance and b is the mean distance for each point to its neighbouring cluster (closest cluster for which the point is not being part). Each point is labelled as being in a cluster using the k-means clustering (with correlation-based Mahalanobis distance), while the distance used in the calculation of a and b is the Euclidean distance. We have computed the Silhouette coefficient for 18 clustering (number of clusters ranging from 2 to 20; Figure 3). As the distribution of the Silhouette coefficient is asymmetric, we sort this sensitivity test using the median. The maximum median Silhouette coefficient gives an optimal number of clusters, which is three in our case (Figure 3a). Therefore, after reintroducing the open-ocean grid cell for each year, we end up with four clusters (three optimal clusters obtained using the Silhouette coefficient for non-zero seasonal cycle of sea ice and the open-ocean cluster reintroduced manually). The code developed for this study is available for download at https://github.com/amelie-simon-pro/SIC_Clustering.



360

361 Figure 3: Boxplot of the Silhouette coefficient for a number of clusters from 2 to 20.
 362 The box extends from the first quartile (0.25) to the third quartile (0.75) of the
 363 Silhouette coefficient. The whiskers indicate the 1st and 99th percentiles. The
 364 green-dashed and orange-solid lines indicate the mean and median values, respectively
 365 (panel a). Equal quantile separation initialization: centroids of the first iteration of the
 366 clustering for a number of cluster of 2, 3 and 4 (panel b)

368 3. Results

369 3.1 Clustering outputs

370

371 The clustering method connects each seasonal cycle to a given cluster (Figure
372 4a) and provides the centroids of each cluster (Figure 4b). As shown in Figure 4a for
373 year 1979 and 2023, the clustering method associates the sea-ice seasonal cycle of
374 each year and each grid cell to the nearest seasonal cycle type (based on the smallest
375 Mahalanobis distance between the seasonal cycle of the point and the seasonal cycle
376 of the centroids). Without giving any information to the clustering algorithm on the
377 spatial and temporal dependency between the seasonal cycles, we retrieve spatially
378 continuous patterns. The clusters are sorted going toward the pole as follows: the
379 open-ocean cluster, the partial winter-freezing cluster, the full winter-freezing cluster
380 and the permanent sea-ice cluster. The first three clusters exhibit wavy bands
381 surrounding the pole, and the permanent sea-ice cluster sits over the pole. More
382 details on the description of the regions will follow based on our probabilistic
383 framework (section 3.2).

384 The centroids (Figure 4b) of a cluster correspond to the average of all seasonal
385 cycles belonging to the cluster. It is referred to as the type of seasonal cycle. They
386 exhibit the expected physical behavior that, due to the thermal inertia of the ice and
387 indirect processes involving the ocean and atmosphere, the maximum sea-ice coverage
388 (in March) follows the minimum solar insolation by a lag of around 3 months, and the
389 minimum sea-ice coverage (in September) occurs around 3 months after the maximum
390 solar insolation (Parkinson et al. 1987).

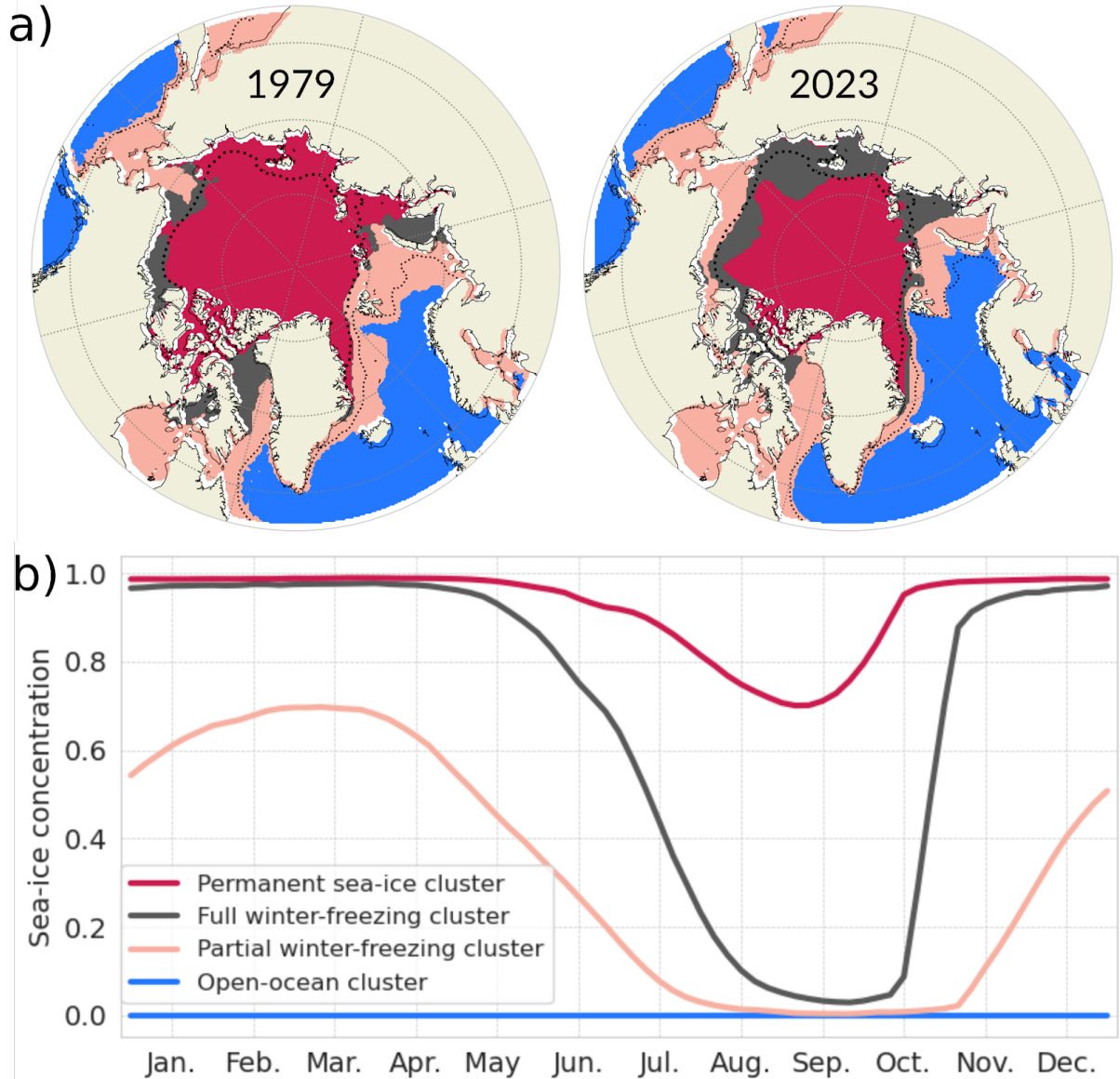
391 The four types of seasonal cycles present different features. The open-ocean
392 cluster has a SIC equal to zero all year round, which was sought for our analysis and
393 represents year-long ice-free conditions. We refer to ice-free conditions when SIC is
394 below 0.15. The second cluster, referred to as partial winter-freezing, has a
395 quasi-sinusoidal shape with a mean SIC ranging from ~70% in March to no-ice in

396 summer (early August to mid-October). The full winter-freezing cluster is bound to a
397 SIC of 100% from mid-November to April and to almost no-ice by mid-September. For
398 this cluster, the sea ice completely melts in 5 months (from April to September) and
399 totally freezes up in 2 months (from mid-September to mid-November). The full
400 winter-freezing cluster has more abrupt seasonal changes compared to the partial
401 winter-freezing cluster. The permanent sea-ice cluster has sea ice covered all year
402 round, with only a partial melting between May and October, peaking at its minimum in
403 late August (mean SIC around 70%).

404

405

406



407

408 Figure 4: (a) Four types of seasonal cycles (output of the clustering method, called
 409 centroids) (b) their corresponding regions for the years 1979 (left) and 2023 (right).
 410 The dotted thin and thick lines are the mean SIC of 0.15 and 0.8 for the period
 411 1979-2023, respectively.

412 This clustering analysis shed light on sea ice precursors for fully covered ice
 413 conditions and ice-free conditions, as the three clusters with sea ice have different first
 414 dates of retreat and first dates of advance. In our optimal data separation analysis, it
 415 appears that when considering areas totally covered by ice in winter (permanent and
 416 full winter freezing clusters), the first date of retreat is a good indicator for ice-free
 417 conditions in summer. Considering a given location fully ice-covered in a given winter,

our clustering results suggest that when the sea ice starts to melt in April, the seasonal cycle belongs to the full winter-freezing cluster and be ice-free the next summer. In contrast, when the melting starts one month later (in May) the seasonal cycle belongs to the permanent sea-ice cluster and the considered location will not be ice-free in summer. Besides, the freezing date for areas free of ice could differentiate between the partial winter-freezing and full winter freezing clusters and subsequently predict full ice conditions in the following winter. In our clustering, a freezing starting in October totally freezes in winter which is not the case if the freezing starts in November, having a maximum of about 70% SIC in March. Therefore, it seems that, for ice-free conditions in summer, the first date of advance is a good indicator for full ice conditions in the next winter.

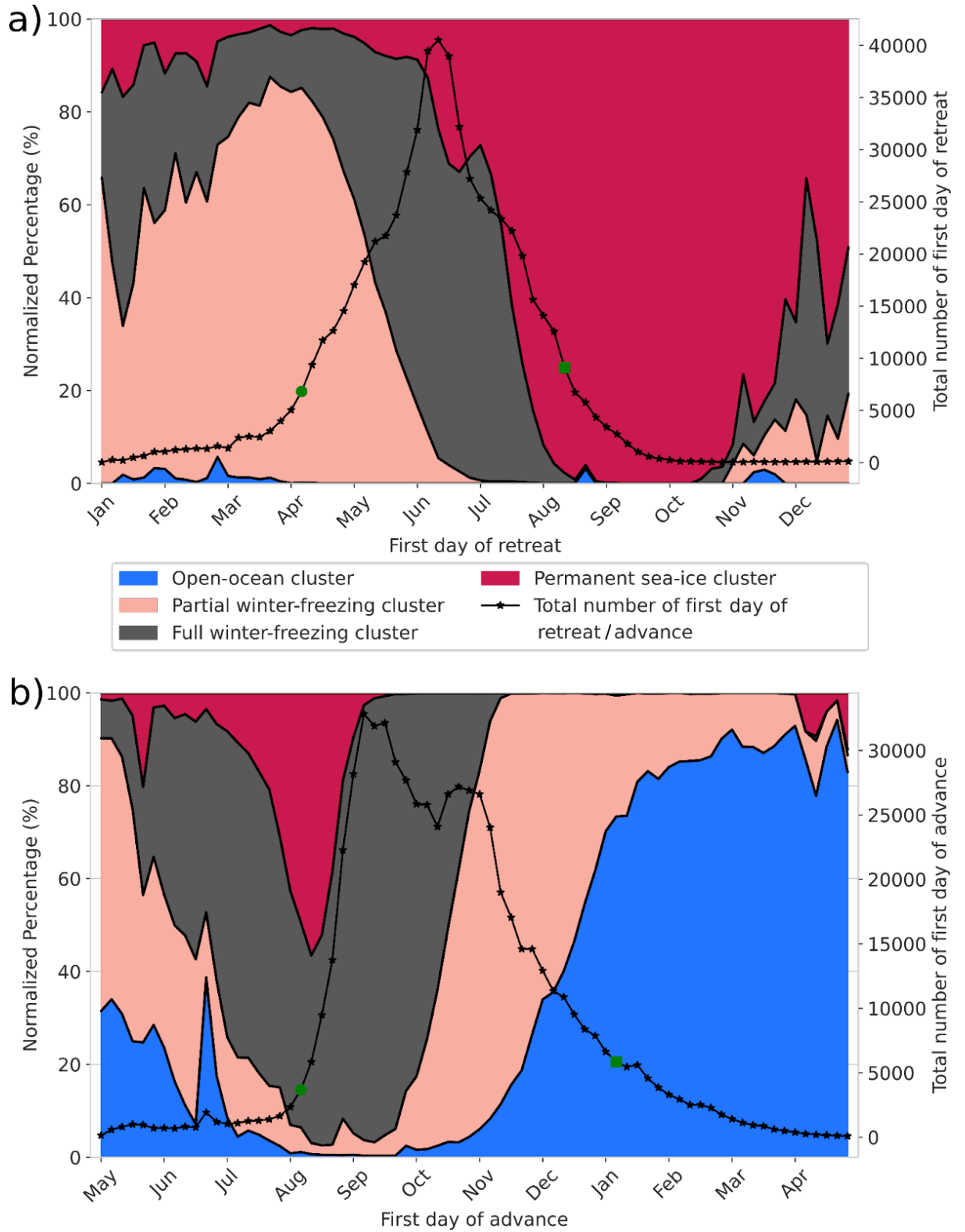
However, this suggestion relies solely on the shape of the four types of seasonal cycles but to properly quantify this, the spread must be taken into account. Figure S3 displays the spread of the seasonal cycle by plotting the quantiles 0.1, 0.5 and 0.9 of each cluster. To verify our hypothesis on sea-ice indicators, we account for the spread of the date of retreat and date of advance for each cluster. To do so, we calculate the first date of retreat (the first date after the maximum SIC that is below 0.9) for each seasonal cycle experiencing fully ice covered conditions (having at least one value above 0.99 during the year). We also calculate the first date of advance (the first date after the minimum SIC that is above 0.1) for each seasonal cycle experiencing ice-free conditions (having at least one value below 0.01 during the year). For these calculations, seasonal cycles have been temporally filtered using a 15 days sliding window in order to get rid of short-term dynamical ice events, as done in Lebrun et al., (2019). To circumvent the effect of the discontinuity between 31 December and 1 January, we define the origin of time in May for the calculation of the date of advance. We then label each first date of retreat and first date of advance for each seasonal cycle with its corresponding cluster according to our clustering analysis (Figure 4a).

The normalized probability over each cluster of the first date of retreat and first date of advance at each date is shown Figure 5. This figure also displays the total number of the first date of retreat and the first date of advance of all clusters for each date. If the first date of retreat occurs between January and April, there is around 95%

449 of chance to belong to either the open-ocean cluster, the partial winter-freezing
450 cluster or full winter freezing cluster, which all present ice-free duration in the
451 following summer. However, this situation did not often occur, as the total first date of
452 retreat happening in this period is unlikely (solely around 5% of first date of retreat for
453 all clusters). The first date of retreat is more likely to occur between the beginning of
454 April and August, as within this period around 90% of the total date of retreat for all
455 clusters exist. A first date of retreat in early July has around 70% of chance to belong to
456 the full winter-freezing cluster which present ice-free conditions in summer while a
457 first date of retreat in early August has around 90% of chance to belong to the
458 permanent sea-ice cluster which doesn't show ice-free conditions in summer.

459 The first date of advance is more likely to occur between the beginning of
460 August until the beginning of January, as within this period around 90% of the total
461 date of advance for all clusters exist. A first date of advance in early September has
462 around 95% of chance to belong to the full winter freezing cluster which present fully
463 ice covered condition in the following winter, while a first date of advance in early
464 November has around 80% of chance to belong to the partial winter-freezing or open
465 ocean clusters which do not show fully ice covered conditions in the following winter.
466 Therefore, this simple model suggests that the first date of retreat could be a good
467 indicator for ice-free conditions the following summer and the first date of advance a
468 good indicator for fully ice cover conditions the following winter.

469



470

471

472

473

474

Figure 5: Normalized probability of the first date of retreat (panel a) and first date of advance (panel b) for each cluster. The solid lines with star markers are the total number of first dates of retreat and first dates of advance for all clusters. The green circle markers (start date) and green square markers (end date) cover the shortest

period where around 90% of the first date of retreat, respectively the first date of advance, for all clusters occurs.

To emphasize the added value of our clustering, we compare it to a more classical classification (Figure 6b) in which the sea ice cover is separated into the packed ice category ($0.8 < \text{SIC} < 1$), the Marginal Ice Zone (MIZ; $0.15 < \text{SIC} < 0.8$) and the remaining, open-ocean category ($\text{SIC} < 0.15$; Aksenov et al. 2017). Using the cluster vision, we compute the evolution of the total area corresponding to each of our four clusters (Figure 6a).

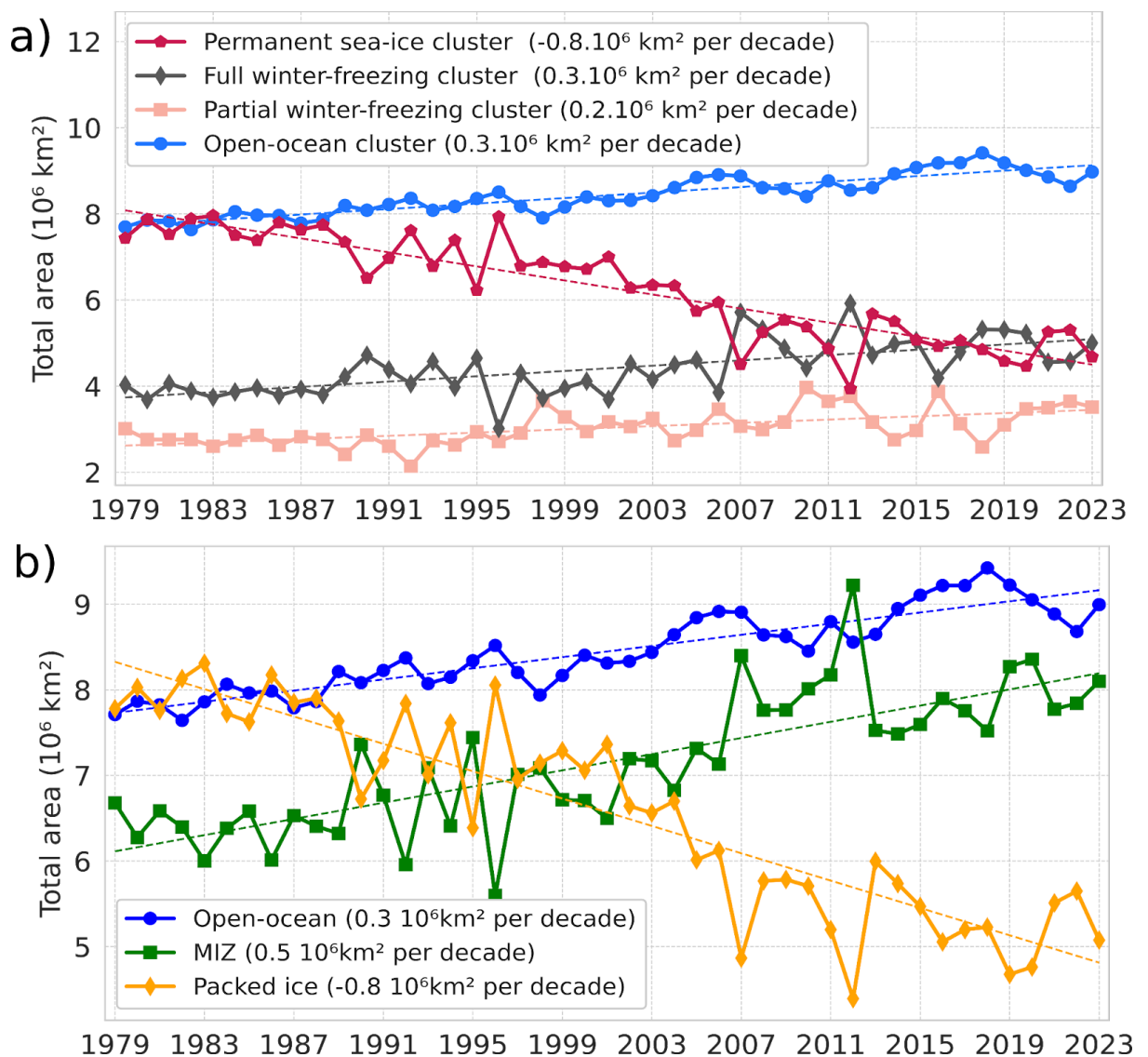


Figure 6: (a) Time series of the total area covered by each of the four clusters. (b) Time series of the area covered by three categories: packed ice ($0.8 < \text{SIC} < 1$), the Marginal Ice Zone (MIZ; $0.15 < \text{SIC} < 0.8$) and the open-ocean ($\text{SIC} < 0.15$). All curves show a

significant linear trend with a p-value less than 0.05 using a Wald Test with a t-distribution.

These two methods (Figure 6a and Figure 6b) both indicate a shift toward more seasonal and ice-free conditions. Indeed, in the clustering method the permanent sea-ice cluster has notably decreased of the same amount than the packed ice in the classical categorization ($-0.8 \cdot 10^6 \text{ km}^2$ per decade). Also, the open-ocean cluster follows the same trend of the open-ocean category ($0.3 \cdot 10^6 \text{ km}^2$ per decade). The increase in the area of MIZ category is around $0.5 \cdot 10^6 \text{ km}^2$ per decade and has been demonstrated previously (Cocetta et al., 2024; Song et al., 2025). Therefore, it appears with our clustering that the MIZ is refined into two clusters : the full winter-freezing ($0.3 \cdot 10^6 \text{ km}^2$ per decade) and the partial winter-freezing cluster ($0.2 \cdot 10^6 \text{ km}^2$ per decade). This suggests that the tendency is more likely to shift to a more abrupt melting and growth seasonal cycle (full winter-freezing cluster) compared to a quasi-sinusoidal sea-ice seasonal cycle (partial winter-freezing cluster) or, in other words, that the tendency is more likely to a total ice cover in winter with a short ice-free season (2 months, full winter-freezing cluster) than a partial ice cover in winter with a long ice-free season (4 months, partial winter freezing cluster).

Also, looking at the years with marked extremes in September sea ice extent, (2007, 2012, 2016 and 2020; see introduction), the MIZ categorization shows a transfer of area between the packed ice and the MIZ. In our clustering vision, 2007, 2012 and 2020 show a transfer of area between the permanent sea-ice cluster and full winter-freezing cluster while 2016 show a transfer of area between the full winter-freezing and the partial winter freezing, reflecting different dynamical changes in the sea-ice seasonal cycles. Therefore, our clustering analysis presents a more detailed description of the MIZ category.

As a given seasonal cycle can be in between two or more seasonal cycle centroids, we introduce the probability to belong to one cluster in the next section.

3.2 Probability to belong to a cluster

3.2.1 Calculation

To calculate the probability P of a grid point to belong to each cluster. We define the vectors \mathbf{x} and $\mathbf{c}(\mathbf{k})$, corresponding respectively to the SIC observed at a grid cell over a year (i.e., 73 intervals of 5 days) and the cluster centroid \mathbf{k} . These are of dimension (73x1) and are written as:

$$\begin{aligned} \mathbf{x} &= [x_1, \dots, x_{73}]^T; \\ \mathbf{c}(\mathbf{k}) &= [c_1(\mathbf{k}), \dots, c_{73}(\mathbf{k})]^T \end{aligned} \quad (1)$$

The Euclidean distance scalar between the point \mathbf{x} and the centroid \mathbf{k} is defined as follows:

$$d_{x,c(k)} = \sqrt{(\mathbf{x} - \mathbf{c}(\mathbf{k}))^T (\mathbf{x} - \mathbf{c}(\mathbf{k}))} \quad (2)$$

The probability P reads:

$$P(x, k) = \left[\sum_{l=1}^{n_c} \left(\frac{d_{x,c(k)}}{d_{x,c(l)}} \right)^2 \right]^{-1} \quad (3)$$

with n_c the total number of clusters (four in our case). P ranges from 0 to 1 and the sum over the four clusters of P equals 1. In other words, the probability of being in a cluster is set by the distance of one seasonal cycle to a seasonal cycle centroid, normalized by the sum of the Euclidean distance to all clusters. This means that we use a “fuzzy” k-means clustering where the assignment is soft (each data point can be a member of multiple clusters) in contrast to a hard or crisp assignment (each data point is assigned to a single cluster; Jain et al., 2010).

We call the total probability, P_t , the normalized area weighted probability over all grid cells. We sum, for each year, the probability weighted by the area of each grid cell over all grid cells divided by the sum of the probability weighted by the area of each grid cell over all clusters and all grid cells. P_t can be written as:

$$Pt(k) = \frac{\sum_x P(x,k) \cdot \text{area}(x)}{\sum_k \sum_x P(x,k) \cdot \text{area}(x)} \quad (4)$$

3.2.2 Trend of the pan-Arctic probability to belong to a cluster

After attributing each point to a probability of belonging to each cluster per year (using equation (4)), we analyze in a spatially integrated way the pan-Arctic evolution of the total probability to belong to a cluster (normalized area-weighted probability). The probability of belonging to the open-ocean cluster is around 40%, to the permanent sea-ice cluster is around 29% and to the full winter-freezing cluster is around 18 % and to the partial winter-freezing cluster is around 13% (Figure 7). Note that the absolute value reflects our choice of domain, here above 55 °N.

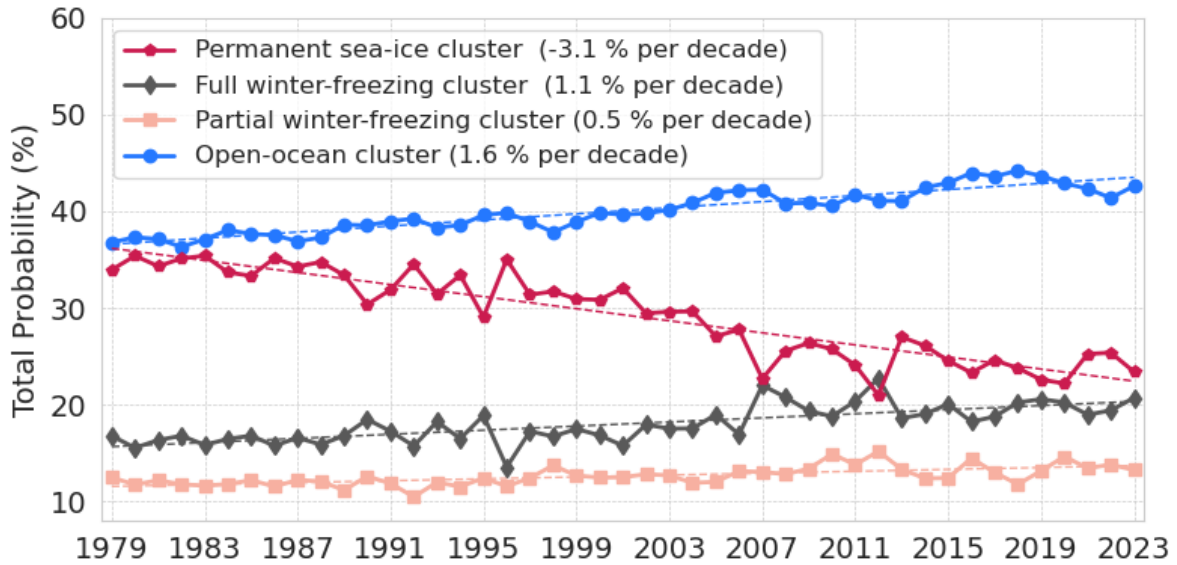


Figure 7: Evolution of the total probability (see Equation (4)) to belong to each cluster. All clusters show a significant linear trend with a p-value less than 0.05 using a Wald Test with a t-distribution

However, the time evolution of these clusters is in direct relation to the dynamics of the Arctic sea ice. A linear regression analysis indicates that the trends for all clusters are statistically significant, with a p-value less than 0.05 using a Wald Test with a t-distribution. The total probability of belonging to the permanent sea-ice cluster overall declines by around 3.1% per decade with an acceleration around the

1997-2012 period. The total probability of the three other clusters shows a decline, firstly for the open-ocean cluster (1.6% per decade) and to a smaller extent full winter-freezing (1.1%) and the partial winter-freezing (0.5% per decade). Therefore, most of the pan-Arctic probability loss over the last 45 years from the permanent sea-ice cluster is compensated by a gain of the open-ocean cluster and to a smaller extent to the full and partial winter-freezing clusters.

3.2.3 Regional probability to belong to a cluster

To analyze spatial redistributions of clusters over time, we average the probability (calculated equation (3)) over three periods of 15 years (Figure 8). During the first period (1979-1993), the Nordic Seas, the Bering Sea and the Gulf of Alaska belonged solely to the open-ocean cluster (free of ice). Going northward, an outer belt shape connecting the southern Barents Sea, the northern and east Greenland Sea and the southern and east Labrador Sea in the Atlantic side and the northern Bering Sea and Sea of Okhotsk mainly belongs to the partial winter-freezing cluster. Further north, an inner belt shape tight to the Arctic coast (Beaufort Sea, Chukchi Sea, East Siberian Sea, Laptev Sea, southern Kara Sea) and to the northern Barents Sea, and Baffin Bay mainly belong to the fully winter-freezing cluster. The central Arctic predominantly belongs to the permanent sea-ice cluster. The edge of the 0.3 probability of belonging to the permanent sea-ice clusters of the period 1979-1993 follows the border of the Marginal Ice Zone (0.8 SIC) located in the Central Arctic. Some regions do not have a dominant cluster but instead have a strong probability of belonging to more than one cluster, such as the northern Kara Sea, the northern Greenland Sea and the Hudson Bay.

In the subsequent periods (1994-2008 and 2009-2023), the open-ocean cluster continuously expanded in the Barents Sea, East Greenland Sea and Labrador Sea. In these same regions, the other three clusters (partial winter-freezing, full winter-freezing and permanent sea ice clusters) retract. The permanent sea-ice cluster exhibits substantial change, with intense shrinking from the Pacific side of the central Arctic, losing areas in a belt shape from the Beaufort Sea to the Laptev Sea which is

mainly gained by the full winter-freezing sea-ice cluster. This indicates increasingly frequent summer ice-free conditions during the 1979-2023 period.

Therefore, spatial redistributions in the clusters occur over time. The permanent sea-ice retraction from the Pacific side is compensated by the full winter-freezing cluster and the open-ocean cluster expansion in the Atlantic side is compensated by loss of the partial winter-freezing cluster.

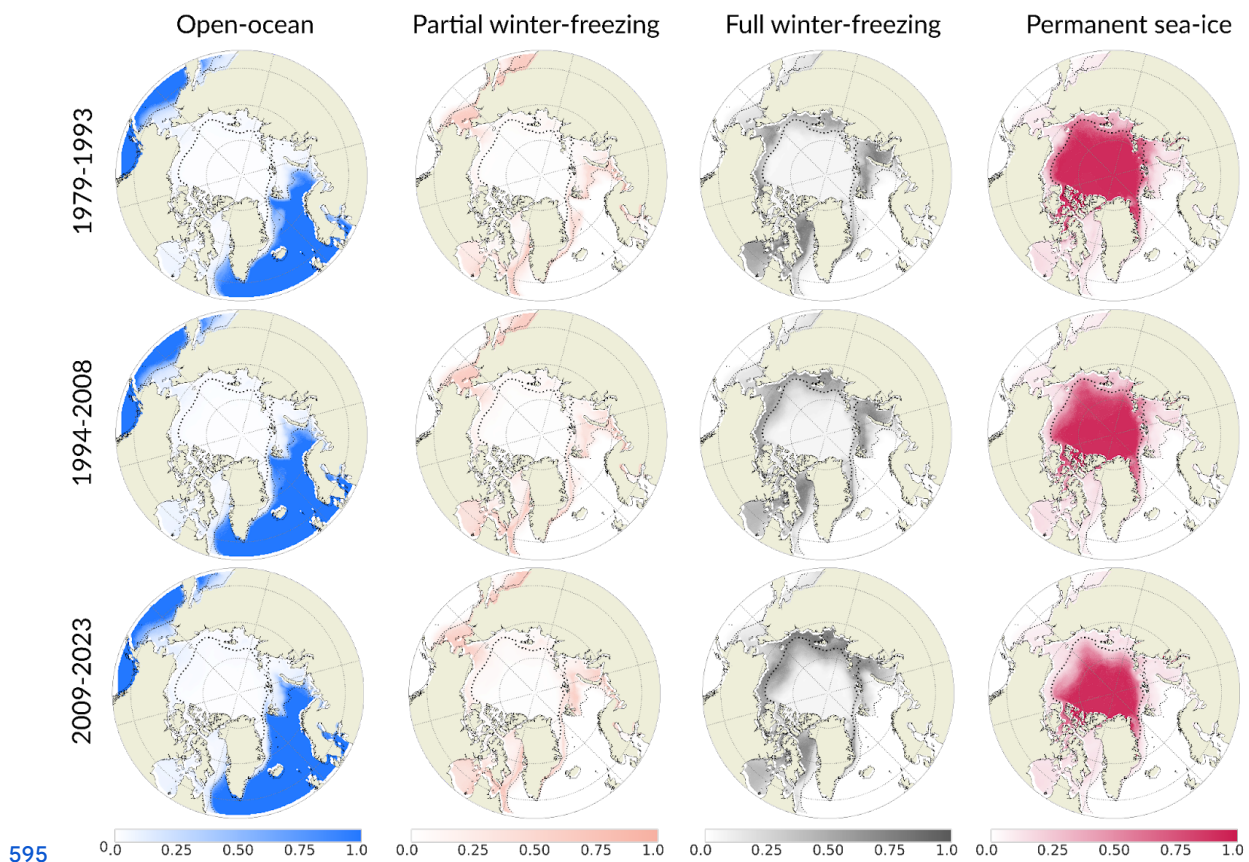
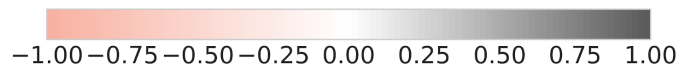
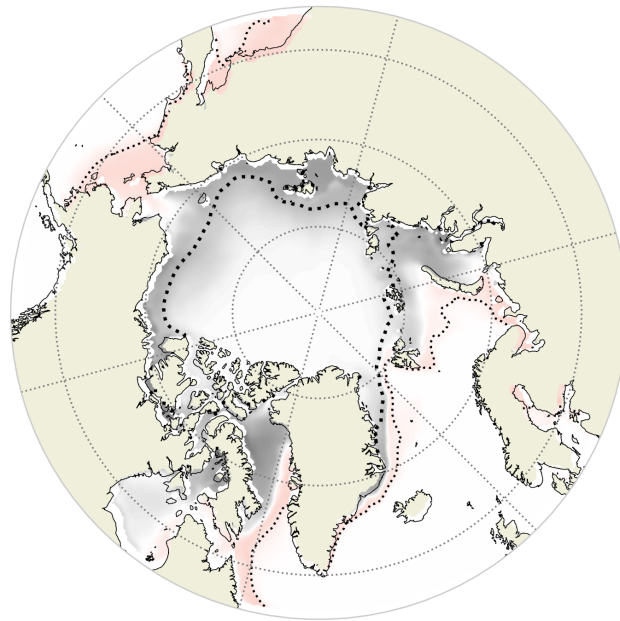


Figure 8: Map of the probability of each cluster: open-ocean (first column), partial winter-freezing (second column), full winter-freezing (third column) and permanent sea-ice (fourth column). Rows correspond to three periods of 15 years: 1979-1993 (top row), 1994-2008 (middle row) and 2009-2023 (bottom row). The dotted thin and thick lines are the mean SIC of 0.15 and 0.8 for the period 1979-2023, respectively. The circle sitting over the north pole is the pole hole (see section 2.1).

Therefore, over the whole period (1979-2023) the open-ocean cluster resides predominantly in the southern part of the Arctic and the permanent sea-ice cluster in

the central Arctic. These two clusters have no or weak seasonal changes (constant zero for open-ocean clusters and variation between 100% and 70% SIC for permanent sea-ice). To better shape our understanding of seasonal cycles which strongly change (from no ice to 70% SIC for the partial winter-freezing clusters and to 100% SIC for the full winter-freezing cluster), we distinguish which areas are mainly associated with each of these two clusters by plotting the difference of probability between these two clusters for the whole period (Figure 9). It displays spatially consistent regions. The inner belt connecting the Baffin Bay to northern Barents is attached to the coastal Arctic and is dominated by the full winter freezing cluster. Further south, this cluster is surrounded by an outer belt from the southern Barents to the southern Labrador Sea and by the Bering Sea dominated by the partial winter-freezing cluster. Thus, the full winter-freezing cluster is more likely to occur in coastal areas than the partial winter-freezing cluster. This spatial repartition might be explained by the difference in year-round shapes of the seasonal cycles: quasi-sinusoidal for partial winter-freezing and asymmetric for full winter-freezing. Indeed, Eisenman (2010) demonstrates that the coastlines, by blocking the sea-ice growth, drive the asymmetric seasonal cycle's shape while sea-ice free to grow and melt (not being blocked by land) has a sinusoidal shape. Our results corroborate this finding.



626

627 Figure 9: Map of the probability of the full winter-freezing cluster minus the partial
 628 winter-freezing cluster averaged over the period 1979-2023. The dotted thin and thick
 629 lines are the mean SIC of 0.15 and 0.8 for the period 1979-2023, respectively.

630

631 3.3 Regime stability and transition

632 In order to describe the grid-cell evolution of the Arctic sea ice over the period
633 1979-2023, we further classify each grid cell into four regimes: stable, unstable,
634 destabilization, and stabilization. First, we define a stable phase as a sequence when
635 the cluster having the maximum probability stays the same for at least 10 years in a
636 row, allowing for a tolerance of 1 year to belong to a different cluster within that
637 period. Sensitivity tests have been performed on this definition (Figure S4), and the
638 results do not change when we apply small definition changes (i.e., 9 to 11 years
639 minimum length of the same cluster with zero to 2 years of tolerance). Second, we label
640 each grid cell as follows:

- 641 1. Grid cells being in a unique stable phase over the whole period
642 (1979-2023) are labelled stable regime;
- 643 2. Grid cells belonging to a stable phase at the end of the period and not
644 being in a stable phase before or being in another stable phase (with a
645 different dominant cluster) before are labelled stabilization;
- 646 3. Grid cells not being in a stable phase at the end of the period and being in
647 a stable phase before are labelled destabilization;
- 648 4. Grid cells not being in a stable phase during the whole period or one or
649 several stable phases between periods of not stable phases are labelled
650 unstable.

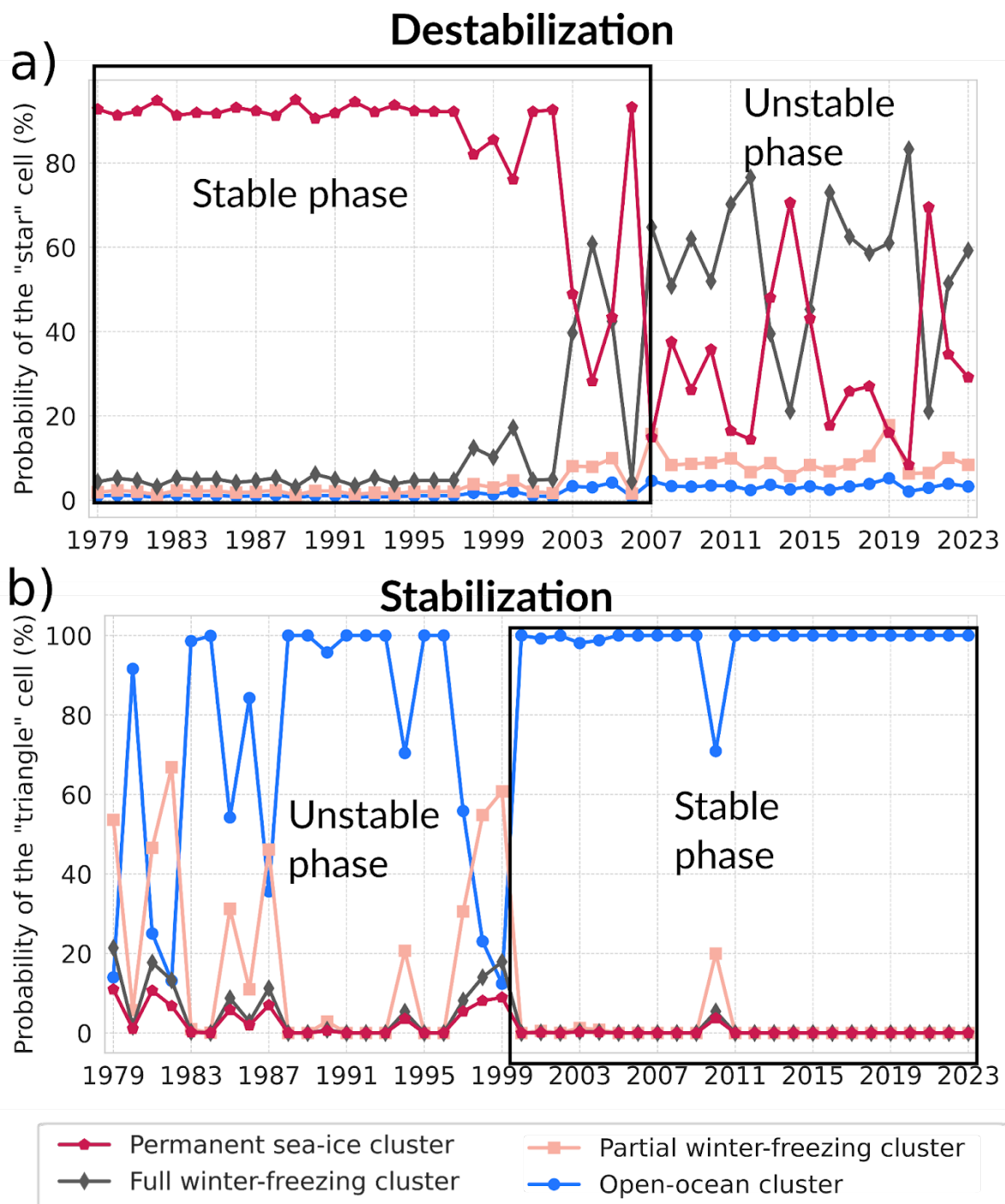
651 Figure 10 illustrates how we define the stabilization and destabilization labels.

652

653

654

655



656

657 Figure 10: Evolution of clusters at the location denoted by the star (a) and the triangle
 658 (b) in Figure 11. The stable phase is delimited by a black rectangle. These locations
 659 have been chosen to illustrate the destabilization and stabilization label of the Arctic
 660 sea ice evolution, respectively.

661

As shown in Figure 11, the stable region predominantly covers the central part of the Arctic Ocean, including the area around the North Pole, following most of the regions covered by permanent sea-ice cluster, as well as the ocean regions in the open-ocean cluster. Smaller regions present stable conditions: the northern Baffin Bay and southeast of Kara Sea dominated by the full winter-freezing cluster and northern Bering Sea associated with the partial winter-freezing cluster (Figure 8). Some regions jump between two or more clusters during the whole period, experiencing an unstable regime. These regions are sparse, the biggest being the northern Barents and Kara Seas. Most unstable regime areas are sitting in between stabilization and destabilization regimes areas.

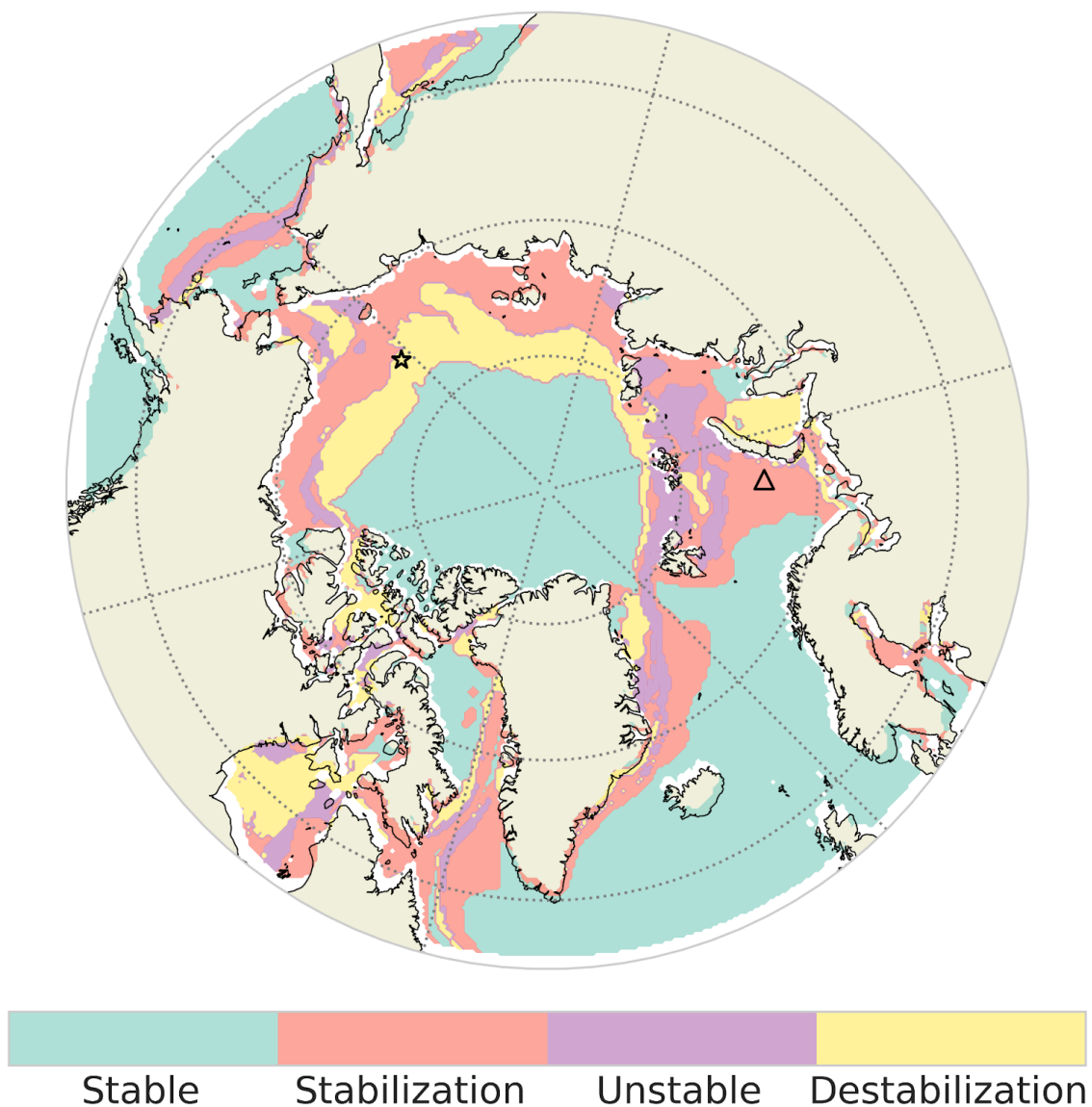


Figure 11: Map of the four regimes (stable, stabilization, unstable, and destabilization) used to describe the evolution of Arctic clusters based on sea-ice seasonal cycles. The star and triangle markers indicated the two localizations used to illustrate the destabilization and stabilization in Figure 10 respectively.

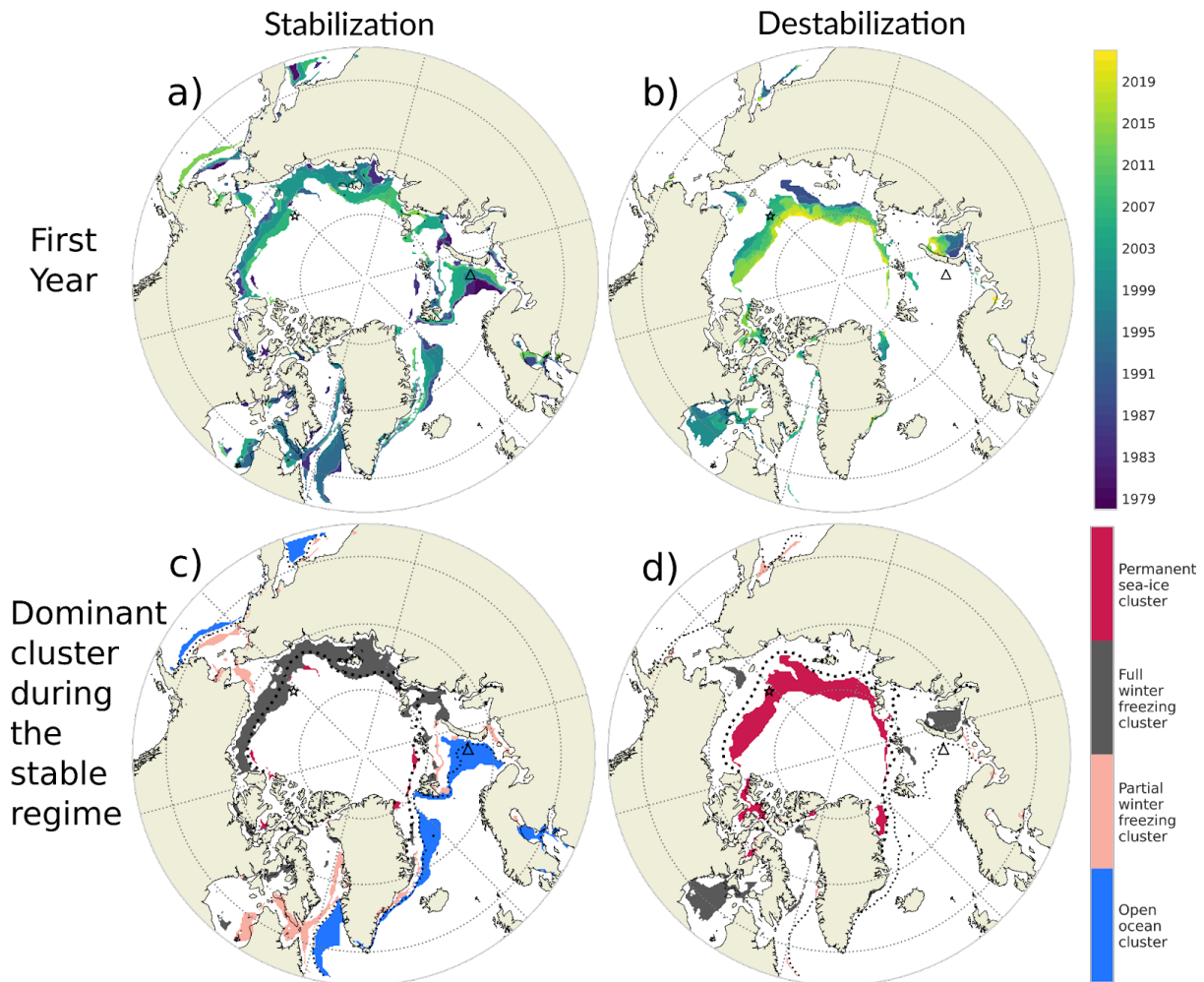
To describe the stabilization and destabilization regimes, we display the dominant cluster (the cluster having the maximum probability) during the stable phase of these two regimes (early period for the destabilization regime and late period for the stabilization period; Figure 12c and 12d). And, to quantify the year of transition, we introduce the year of stabilization as the first year when the stable phase occurs until the end of the whole period (Fig. 12a), and the year of destabilization as the last year of the stable phase (Fig. 12b). One should note that according to our definition the maximum year of stabilization is 2013 and minimum year of destabilization is 1989.

An inner belt shape (from southern Beaufort Sea to the southern Kara) connecting parts of the Barents Sea and around Greenland (Greenland Sea and Labrador Sea) is labeled stabilization (Figure 11). The inner belt shape stabilized to the full winter-freezing cluster while the other regions in the Atlantic side (Barents to Labrador Sea) stabilized to the open-ocean cluster (Figure 12c). This is in link with the shift of the permanent sea-ice cluster to the full winter freezing cluster in the Pacific side and the expansion of the open-ocean cluster in the Atlantic side (Figure 8). This transition occurred in a northward propagation starting in the 80's in the Barents Sea for the Atlantic side and in the Laptev in for the Pacific side (Figure 12a).

The belt from the northern Canadian Archipelago to the northern Greenland Sea (wider from the Beaufort Sea to Laptev Sea) is in the destabilization regime. These regions lost their typical permanent sea-ice cluster (Figure 12d) being mainly replaced by the full winter freezing cluster (Figure 8) in a northward propagation. The southeast Kara Sea and Hudson Bay, in a northward propagation for the former and during the 2000's for the Hudson Bay (Figure 12b).

702 In summary, the four regimes illustrate how different regions of the Arctic have
 703 experienced changes in stability. This regionalization suggests a more latitudinal vision
 704 of the region, as for the Seas from the Beaufort to the Kara Seas, the southern parts is
 705 experiencing a stabilization to a new cluster and the northern part a destabilization of
 706 an old cluster.

707



708

709 Figure 12: First year of stabilization (a) and destabilization (b) and associated dominant
 710 cluster for the stable regime of the stabilization (c) and destabilization (d). The star and
 711 triangle markers indicated the two localizations used to illustrate the destabilization
 712 and stabilization in Figure 10, respectively.

713 4. Conclusion and Discussion

714 This paper explores the use of a data-driven method using satellite observation
715 of SIC to study the spatio-temporal evolution of sea ice in the Arctic over the period
716 1979-2023. We determine Arctic regions based on statistically different sea-ice
717 seasonal cycles, and describe Arctic changes through the time evolving borders. The
718 methodology is based on the clustering (machine learning method) of the full sea-ice
719 seasonal cycle, instead of classic descriptors used in previous studies (e.g., sea-ice
720 extent, Marginal Ice Zone, sea-ice age and ice-free duration). It shows that the Arctic
721 sea ice changes are best described with four clusters of seasonal cycles: the
722 open-ocean cluster (with no ice during the whole year), the permanent sea-ice cluster
723 (total sea-ice coverage with a minimum of 70% SIC in September), and two clusters
724 showing ice-free conditions in late summer, namely the partial winter-freezing cluster
725 and the full winter-freezing cluster. The full winter-freezing cluster has a larger SIC in
726 winter, displays a more abrupt summer melting and winter freezing and has a shorter
727 ice-free season than the partial winter-freezing one. The central Arctic belongs to the
728 permanent sea-ice cluster. According to this clustering, a first date of retreat in early
729 July has around 70% of chance to belong to the full winter-freezing cluster which
730 shows ice-free conditions in summer. A first date of advance in early September has
731 around 95% of chance to belong to the full winter freezing cluster which presents fully
732 ice covered condition in the following winter.

733 Another important aspect of our analysis is that a given seasonal cycle can be in
734 between two or more seasonal cycle centroids. We therefore believe that a
735 probabilistic view when dealing with clustering is important. By analysis the evolution
736 of the pan-Arctic clusterings over the 1979-2023 period, we show that the probability
737 to belong to the permanent sea-ice seasonal cycle has decreased by 3.1 %/decade
738 which is compensated with an increase of probability to belong to the open-ocean
739 cluster (1.6 % per decade), the full winter freezing cluster (1.1 % per decade) and to a
740 smaller extent to the partial winter-freezing cluster (0.5 % per decade). Regional shift
741 in the clusters occurs over time. In general, the permanent sea-ice retraction from the
742 Pacific side is compensated by the full winter-freezing cluster and the open-ocean

cluster expansion in the Atlantic side is compensated by loss of the partial winter-freezing cluster.

The added value of our description compared to the MIZ category (sea-ice concentration between 0.15 and 0.8) is the new classes of partial and full winter freezing. This could be important for sea-ice dynamics and forecasting understanding. Our result suggests that the trend is primarily controlled by the trend of the more abrupt melting and growth seasonal cycle (full winter-freezing cluster) compared to the trend of the quasi-sinusoidal sea-ice seasonal cycle (partial winter-freezing cluster) or, in other words, that the trend is more likely due to increase of regions with total ice cover in winter with a short ice-free season (2 months, full winter-freezing cluster) than increase of regions with a partial ice cover in winter with a long ice-free season (4 months, partial winter freezing cluster).

We introduce another diagnostic to quantify the regime stability and transition of the Arctic sea ice. The stable region (having always the same dominant cluster for the whole period 1979-2023) predominantly covers the central part of the Arctic Ocean, including the area around the North Pole, following most of the regions covered by permanent sea-ice cluster, as well as the ocean regions in the open-ocean cluster. Smaller regions present stable conditions: the northern Baffin Bay and southeast of Kara Sea dominated by the full winter-freezing cluster and northern Bering Sea associated with the partial winter-freezing cluster. From the Beaufort to the Kara Seas, the southern parts have stabilized (experiencing a new typical seasonal cycle, corresponding to the full winter-freezing cluster) and the northern part have destabilized (losing their typical permanent sea-ice seasonal cycle).

This regionalization suggests a more latitudinal vision of the region. Also, this study calls for pan-Arctic sea-ice thickness observation in order to better understand sea-ice changes.

5. Discussion

The k-means clustering of the sea-ice seasonal cycle we applied to the Arctic shares similarities with the analysis of Wachter et al. (2021) for the Antarctic. The main

773 differences however reside in our use of Mahalanobis distances, to account for the
774 correlation between the months, and the initialization based on equal separation of
775 quantiles for the centroids, to avoid any random aspect in the clustering algorithm.
776 These two choices enable to constrain the clustering with physical features. Besides,
777 by the use of the Silhouette coefficient, we found the Arctic is best described with a
778 number of clusters of 3 (the open-ocean has been added afterward). This number has
779 also been found by Fuckar et al., (2016) using a suite of indices (Krzanowski-Lai,
780 Calinski-Harabasz, Duda-Hart J index, Ratkowsky-Lance, Ball-Hall, point-biserial, gap
781 statistic, McClain-Rao, tau and scatter-distance index) onto detrended sea-ice
782 thickness of an ocean-sea ice general circulation model. In contrast with Fuckar et al.,
783 (2016) that calculated time series of occurrences of clusters based on the resemblance
784 of the pan-Arctic pattern, our probabilistic method defines a time series of probability
785 of occurrence of each cluster at the grid cell scale. This enables us to study the spatial
786 evolution of the cluster areas, and therefore define spatio-temporal regions that share
787 a common feature (in our case sea-ice seasonal cycle).

788

789 Our clustering approach is complementary to diagnostics involving the dates of
790 melting and freezing onsets, which have been used to quantify changes in the duration
791 and shift of ice-free seasons at the pan or regional Arctic scales (Markus et al., 2009;
792 Stammerjohn et al., 2012; Parkinson 2014; Johnson & Eicken, 2016; Stroeve et al.,
793 2014; Lebrun et al., 2019). Instead, our method enables us to target regions
794 experiencing a redistribution to another typical seasonal cycle representing longer and
795 ice-free seasons, and retrieve the year of the shift. Another advantage is that we do not
796 use any arbitrary cutoff of SIC. Additionally, our diagnostic delimits regions with the
797 same sea-ice seasonal dynamics. The major drawback of our approach resides in the
798 exact grid point quantification of the real seasonal cycle features (such as ice-free
799 duration), as we gather grid cells within a type represented by a single seasonal cycle
800 (the centroid). However, considering the full seasonal cycle gives useful information, as
801 its derivative gives the period of melting and growth. Therefore, the two diagnostics
802 complement each other nicely.

803 By doing the diagnostic of the trend in the length of the sea-ice season for the
804 period 1979-2013, Parkinson (2014) shows that the length of the ice season has
805 shortened in almost all the coastal regions (around -10 days/decade with a maximum
806 -30 days/decade in the northern Chukchi Sea and around -50 days/decade in the
807 northern Barents Sea), the main exceptions being the Bering Sea, portions of the
808 Canadian Archipelago (around +10 days/decade) and the central Arctic where the
809 sea-ice season duration remain unchanged over the period. Similar features are
810 obtained in Lebrun et al., (2019) who considered the period up to 2015. Also, Lukovich
811 and Barber (2007) examination of spatial coherence in SIC anomalies indicates that
812 maximum SIC anomalies prevail near the Kara Sea, Beaufort Sea, and Chukchi Sea
813 regions during late summer/early fall from 1979 to 2004. All these studies are
814 consistent with our results showing a decrease in probability for the permanent
815 sea-ice cluster of about 3.1% per decade, especially in coastal regions of the Pacific
816 side of the Arctic, leading to a shortening of the seasonal cycle. Moreover, we were
817 able to show that this regime transition occurs in a smooth northward propagation.

818 Our clustering approach suggests that the first date of freezing and advance
819 could be key for predicting ice conditions around 6 months in advance. This feature
820 follows a physical behaviour of sea-ice shown by Stammerjohn (2012) and Stroeve et
821 al. (2016). They found strong correlations between the dates of the spring sea-ice
822 retreat and subsequent autumn sea-ice advance (i.e., over the summer), indicating that
823 an early sea-ice retreat is often followed by a late autumn sea-ice advance and
824 conversely, a late sea-ice retreat is often followed by an early autumn sea-ice advance.
825 Indeed, consistent with our clustering analysis, the partial winter-freezing cluster has
826 an early sea-ice retreat (in March) and late autumn sea-ice advance (mid-October)
827 while the full winter-freezing cluster has a late sea-ice retreat (in April) and early
828 autumn sea-ice advance (mid-September). Therefore, this simple model suggests that
829 the first date of retreat could be a good indicator for ice-free conditions the following
830 summer and the first date of advance a good indicator for fully ice cover conditions the
831 following winter. A redefined model which quantifies this without taking into accounts
832 specified clustering is out of the scope of the study. An example of such studies has
833 been done in the Antarctic and shows that at interannual timescales, retreat date
834 anomalies are constrained by seasonal maximum ice thickness (Himminch et al., 2025)

835 and the advance date is controlled by the timing of sea-ice retreat through heat stored
836 in the summer ocean mixed layer (Himmich et al., 2023). In the Arctic, Gregory et al.,
837 2020 by setting up a complex network statistical approach, shows good predictive
838 skills for regional September SIE from previous June SIC, especially toward the Pacific
839 sector.

840 Concerning the growth and melting of sea-ice, Parkinson et al., 1999 and
841 Parkinson and Cavalieri, 2008 showed that the seasonal decay of sea ice extent is
842 gradual during early summer and then accelerates during the remaining summer
843 months, whereas wintertime growth is most rapid in early winter. A standard
844 explanation suggests that this asymmetry between seasonal growth and decay is
845 caused by rapid temperature changes driven by air masses from the Eurasian continent
846 (Peixoto and Oort, 1992). Here this asymmetry in the seasonal cycle is seen only for
847 the permanent sea-ice cluster and full winter freezing cluster, suggesting that the
848 partial winter sea-ice is driven by another driver. The full winter-freezing cluster (with
849 no sinusoidal feature) is more likely present along the Arctic coastline than the partial
850 winter-freezing cluster (with a sinusoidal feature). The reason for this spatial
851 repartition could be explained by the fact that the sinusoidal feature of the sea-ice
852 seasonal cycle is linked to the ability of the ice to freeze and expand freely, without
853 being blocked by land, as suggested by Eisenman (2010).

854 A limitation of the study is the fact that the method accounts solely for the area
855 between the centroid and the seasonal cycles to define the clusters, meaning that
856 there is no constraint to have the same maximum and minimum to belong to one
857 cluster. However, if the shift of minimum or maximum is large, the area will largely
858 increase which prevents having a large discrepancy between the maximum and
859 minimum of the seasonal cycles and their respective centroids. Another limitation of
860 this study is that sea-ice dynamics are analysed using SIC rather than sea-ice volume
861 (which would better represent sea-ice behaviour, including growth and melting), due to
862 the lack of robust and long-term sea-ice thickness data.

863 The introduction in this paper of the clustering of the Arctic sea-ice seasonal
864 cycle, with its statistical aspect, can provide an approach to validate the dynamics of
865 sea-ice in climate models. Indeed, applying the clustering method described here to

models could inform if a given model has the same number of optimal clusters and the types of seasonal cycles as the one obtained from observations. It could also be used to answer how different clusters will be distributed for different future scenarios. Overall, this methodology is transposable to other variables to better answer its past and future variability in a robust statistical framework. These research findings which are relevant for climate models and process understanding, can also provide useful information for forecast application, guiding ecosystem conservation efforts, and thus related policy-making planning.

Author's contribution

All authors contributed to the conceptual design of the study and the interpretation of the results. AS, PT, and FS established the methodological framework. AS developed the code, generated the figures, and drafted the initial version of the article. PT, FS, and CL carefully revised the paper contributing to its improvement.

Financial support

This study is funded by ANR and France 2030 through the project CLIMArcTIC (grant ANR-22-POCE-0005)

Competing interests

The contact author has declared that none of the authors has any competing interests.

Code and data availability

The code developed for this study (clustering, diagnostics and plots) is available for download at https://github.com/amelie-simon-pro/SIC_Clustering. We utilized Mistral (<https://chat.mistral.ai/chat>) and ChatGPT (<https://chat.openai.com/>) to assist in generating small portions of the code, which we subsequently adapted for our script. The daily SIC satellite data from the National Snow and Ice Data Center (NSIDC) are openly available and can be found at <https://doi.org/10.7265/efmz-2t65> (Meier et al., 2021)

Acknowledgement

We enthusiastically thank the four reviewers for their very constructive comments that helped to improve the paper.

901 For the purpose of Open Access, a CC-BY public copyright licence has been applied by
902 the authors to the present document and will be applied to all subsequent versions up
903 to the Author Accepted Manuscript arising from this submission

904

905 References

- 906 Aksenov, Y., Popova, E. E., Yool, A., Nurser, A. G., Williams, T. D., Bertino, L., & Bergh, J.
907 (2017). On the future navigability of Arctic sea routes: High-resolution projections of
908 the Arctic Ocean and sea ice. *Marine Policy*, 75, 300-317.
- 909
- 910 Ardyna, M., & Arrigo, K. R. (2020). Phytoplankton dynamics in a changing Arctic Ocean.
911 *Nature Climate Change*, 10(10), 892-903.
- 912
- 913 Bushuk, M., Ali, S., Bailey, D. A., Bao, Q., Batté, L., Bhatt, U. S., ... & Zhang, Y. (2024).
914 Predicting September Arctic Sea Ice: A Multi-Model Seasonal Skill Comparison.
915 *Bulletin of the American Meteorological Society*.
- 916
- 917 Cavalieri, D. J., Gloersen, P., & Campbell, W. J. (1984). Determination of sea ice
918 parameters with the Nimbus 7 SMMR. *Journal of Geophysical Research: Atmospheres*,
919 89(D4), 5355-5369.
- 920
- 921 Chripko, S., Msadek, R., Sanchez-Gomez, E., Terray, L., Bessi res, L., & Moine, M. P.
922 (2021). Impact of reduced arctic sea ice on northern hemisphere climate and weather
923 in autumn and winter. *Journal of Climate*, 34(14), 5847-5867.
- 924
- 925 Cocetta, F., Zampieri, L., Selivanova, J., & Iovino, D. (2024). Assessing the
926 representation of Arctic sea ice and the marginal ice zone in ocean–sea ice reanalyses.
927 *The Cryosphere*, 18(10), 4687-4702.
- 928
- 929 Cohen, J., Zhang, X., Francis, J., Jung, T., Kwok, R., Overland, J., Ballinger, T. J., Bhatt, U.
930 S., Chen, H. W., Coumou, D., Feldstein, S., Gu, H., Handorf, D., Henderson, G., Ionita, M.,
931 Kretschmer, M., Laliberte, F., Lee, S., Linderholm, H. W., and Yoon, J.: Divergent
932 consensus on Arctic amplification influence on mid-latitude severe winter weather,
933 *Nat. Clim. Change*, 10, 20–29, <https://doi.org/10.1038/s41558-019-0662-y>, 2020
- 934
- 935 Comiso, J. C. (1986). Characteristics of Arctic winter sea ice from satellite
936 multispectral microwave observations. *Journal of Geophysical Research: Oceans*,
937 91(C1), 975-994.
- 938
- 939 Cvijanovic, I., Simon, A., Levine, X., White, R., Ortega, P., Donat, M., ... & Petrova, D.
940 (2025). Arctic sea-ice loss drives a strong regional atmospheric response over the
941 North Pacific and North Atlantic on decadal scales. *Communications Earth &*
942 *Environment*, 6(1), 154.
- 943
- 944 Delhay , S., Massonnet, F., Fich fet, T., Msadek, R., Terray, L., & Screen, J. (2024).
945 Dominant role of early winter Barents–Kara sea ice extent anomalies in subsequent

946 atmospheric circulation changes in CMIP6 models. *Climate Dynamics*, 62(4),
947 2755-2778.

948

949 Deser, C., Tomas, R. A., and Sun, L. (2015). The role of ocean–atmosphere coupling in
950 the zonal-mean atmospheric response to Arctic sea-ice loss, *J. Climate*, 28,
951 2168–2186.

952

953 d'Ortenzio, F., & Ribera d'Alcalà, M. (2009). On the trophic regimes of the
954 Mediterranean Sea: a satellite analysis. *Biogeosciences*, 6(2), 139-148.

955

956 Eisenman, I. (2010). Geographic muting of changes in the Arctic sea ice cover.
957 *Geophysical Research Letters*, 37(16).

958

959 Eyring, V., N.P. Gillett, K.M. Achuta Rao, R. Barimalala, M. Barreiro Parrillo, N. Bellouin,
960 C. Cassou, P.J. Durack, Y. Kosaka, S. McGregor, S. Min, O. Morgenstern, and Y. Sun,
961 2021: Human Influence on the Climate System. In *Climate Change 2021: The Physical*
962 *Science Basis. Contribution of Working Group I to the Sixth Assessment Report of the*
963 *Intergovernmental Panel on Climate Change* [Masson-Delmotte, V., P. Zhai, A. Pirani,
964 S.L. Connors, C. Péan, S. Berger, N. Caud, Y. Chen, L. Goldfarb, M.I. Gomis, M. Huang, K.
965 Leitzell, E. Lonnoy, J.B.R. Matthews, T.K. Maycock, T. Waterfield, O. Yelekçi, R. Yu, and B.
966 Zhou (eds.)]. Cambridge University Press, Cambridge, United Kingdom and New York,
967 NY, USA, pp. 423–552, doi:10.1017/9781009157896.005.

968

969 Forster, P., T. Storelvmo, K. Armour, W. Collins, J.-L. Dufresne, D. Frame, D.J. Lunt, T.
970 Mauritsen, M.D. Palmer, M. Watanabe, M. Wild, and H. Zhang, 2021: The Earth's
971 Energy Budget, Climate Feedbacks, and Climate Sensitivity. In *Climate Change 2021:*
972 *The Physical Science Basis. Contribution of Working Group I to the Sixth Assessment*
973 *Report of the Intergovernmental Panel on Climate Change* [Masson-Delmotte, V., P.
974 Zhai, A. Pirani, S.L. Connors, C. Péan, S. Berger, N. Caud, Y. Chen, L. Goldfarb, M.I.
975 Gomis, M. Huang, K. Leitzell, E. Lonnoy, J.B.R. Matthews, T.K. Maycock, T. Waterfield, O.
976 Yelekçi, R. Yu, and B. Zhou (eds.)]. Cambridge University Press, Cambridge, United
977 Kingdom and New York, NY, USA, pp. 923–1054, doi:10.1017/9781009157896.009.

978

979 Fox-Kemper, B., H.T. Hewitt, C. Xiao, G. Aðalgeirsdóttir, S.S. Drijfhout, T.L. Edwards,
980 N.R. Golledge, M. Hemer, R.E. Kopp, G. Krinner, A. Mix, D. Notz, S. Nowicki, I.S. Nurhati,
981 L. Ruiz, J.-B. Sallée, A.B.A. Slangen, and Y. Yu, 2021: Ocean, Cryosphere and Sea Level
982 Change. In *Climate Change 2021: The Physical Science Basis. Contribution of Working*
983 *Group I to the Sixth Assessment Report of the Intergovernmental Panel on Climate*
984 *Change* [Masson-Delmotte, V., P. Zhai, A. Pirani, S.L. Connors, C. Péan, S. Berger, N.
985 Caud, Y. Chen, L. Goldfarb, M.I. Gomis, M. Huang, K. Leitzell, E. Lonnoy, J.B.R.
986 Matthews, T.K. Maycock, T. Waterfield, O. Yelekçi, R. Yu, and B. Zhou (eds.)]. Cambridge
987 University Press, Cambridge, United Kingdom and New York, NY, USA, pp. 1211–1362,
988 doi:10.1017/9781009157896.011.

989

990 Fučkar, N. S., Guemas, V., Johnson, N. C., Massonnet, F., & Doblas-Reyes, F. J. (2016).
991 Clusters of interannual sea ice variability in the northern hemisphere. *Climate*
992 *Dynamics*, 47(5), 1527–1543. <https://doi.org/10.1007/s00382-015-2917-2>

993

994 Galley, R. J., Else, B. G. T., Prinsenberg, S. J., Babb, D., & Barber, D. G. (2013). Summer
 995 sea ice concentration, motion, and thickness near areas of proposed offshore oil and
 996 gas development in the Canadian Beaufort Sea—2009. *Arctic*, 105-116.

997
 998 GEBCO Compilation Group. (2024). GEBCO 2024 Grid.
 999 doi:10.5285/1c44ce99-0a0d-5f4f-e063-7086abc0ea0f . Date Accessed: 6 Feb. 2025

1000
 1001 Goosse, H., Kay, J. E., Armour, K. C., Bodas-Salcedo, A., Chepfer, H., Docquier, D., ... &
 1002 Vancoppenolle, M. (2018). Quantifying climate feedbacks in polar regions. *Nature*
 1003 *communications*, 9(1), 1919.

1004
 1005 Gregory, W., Tsamados, M., Stroeve, J., & Sollich, P. (2020). Regional September sea ice
 1006 forecasting with complex networks and Gaussian processes. *Weather and Forecasting*,
 1007 35(3), 793-806.

1008
 1009 Gregory, W., Stroeve, J., & Tsamados, M. (2022). Network connectivity between the
 1010 winter Arctic Oscillation and summer sea ice in CMIP6 models and observations. *The*
 1011 *Cryosphere*, 16(5), 1653-1

1012
 1013 Gulev, S.K., P.W. Thorne, J. Ahn, F.J. Dentener, C.M. Domingues, S. Gerland, D. Gong,
 1014 D.S. Kaufman, H.C. Nnamchi, J. Quaas, J.A. Rivera, S. Sathyendranath, S.L. Smith, B.
 1015 Trewin, K. von Schuckmann, and R.S. Vose, 2021: Changing State of the Climate
 1016 System. In *Climate Change 2021: The Physical Science Basis. Contribution of Working*
 1017 *Group I to the Sixth Assessment Report of the Intergovernmental Panel on Climate*
 1018 *Change* [Masson-Delmotte, V., P. Zhai, A. Pirani, S.L. Connors, C. Péan, S. Berger, N.
 1019 Caud, Y. Chen, L. Goldfarb, M.I. Gomis, M. Huang, K. Leitzell, E. Lonnoy, J.B.R.
 1020 Matthews, T.K. Maycock, T. Waterfield, O. Yelekçi, R. Yu, and B. Zhou (eds.)]. Cambridge
 1021 University Press, Cambridge, United Kingdom and New York, NY, USA, pp. 287–422,
 1022 doi:10.1017/9781009157896.004.

1023
 1024 Himmich, K., Vancoppenolle, M., Madec, G., Sallée, J. B., Holland, P. R., & Lebrun, M.
 1025 (2023). Drivers of Antarctic sea ice advance. *Nature Communications*, 14(1), 6219.

1026
 1027 Himmich, K., Vancoppenolle, M., Stammerjohn, S., Bocquet, M., Madec, G., & Fleury, S.
 1028 (2025). Local drivers of Antarctic spring sea ice retreat. *Geophysical Research Letters*,
 1029 52(10), e2025GL114764.

1030
 1031 Huntington, H. P., Quakenbush, L. T. & Nelson, M. (2017). Evaluating the effects of
 1032 climate change on indigenous marine mammal hunting in northern and western alaska
 1033 using traditional knowledge. *Front. Mar. Sci.* 4, 319

1034
 1035 Houghton, I. A., & Wilson, J. D. (2020). El Niño detection via unsupervised clustering of
 1036 Argo temperature profiles. *Journal of Geophysical Research: Oceans*, 125,
 1037 e2019JC015947. <https://doi.org/10.1029/2019JC015947>

1038
 1039 Huntington, H. P., Danielson, S. L., Wiese, F. K., Baker, M., Boveng, P., Citta, J. J., ... &
 1040 Wilson, C. (2020). Evidence suggests potential transformation of the Pacific Arctic
 1041 ecosystem is underway. *Nature Climate Change*, 10(4), 342-348.

1042
1043 IPCC, 2019: Summary for Policymakers. In: IPCC Special Report on the Ocean and
1044 Cryosphere in a Changing Climate [H.-O. Pörtner, D.C. Roberts, V. Masson-Delmotte, P.
1045 Zhai, M. Tignor, E. Poloczanska, K. Mintenbeck, A. Alegría, M. Nicolai, A. Okem, J.
1046 Petzold, B. Rama, N.M. Weyer (eds.)]. Cambridge University Press, Cambridge, UK
1047 and New York, NY, USA, pp. 3–35. <https://doi.org/10.1017/9781009157964.001>.
1048
1049 IPCC, 2021: Summary for Policymakers. In: Climate Change 2021: The Physical
1050 Science Basis. Contribution of Working Group I
1051 to the Sixth Assessment Report of the Intergovernmental Panel on Climate Change
1052 [Masson-Delmotte, V., P. Zhai, A. Pirani, S.L.
1053 Connors, C. Péan, S. Berger, N. Caud, Y. Chen, L. Goldfarb, M.I. Gomis, M. Huang, K.
1054 Leitzell, E. Lonnoy, J.B.R. Matthews, T.K.
1055 Maycock, T. Waterfield, O. Yelekçi, R. Yu, and B. Zhou (eds.)]. Cambridge University
1056 Press, Cambridge, United Kingdom and New
1057 York, NY, USA, pp. 3–32, doi:10.1017/9781009157896.001.
1058
1059 Jain, A. K. (2010). Data clustering: 50 years beyond K-means. *Pattern recognition letters*,
1060 31(8), 651–666.
1061
1062 Jambudi T, Gandhi S (2022) An Effective Initialization Method Based on Quartiles for
1063 the K-means Algorithm. *Indian Journal of Science and Technology* 15(35): 1712–1721.
1064 <https://doi.org/10.17485/IJST/v15i35.714>
1065
1066 Johannessen, O. M., Kuzmina, S. I., Bobylev, L. P., & Miles, M. W. (2016). Surface air
1067 temperature variability and trends in the Arctic: new amplification assessment and
1068 regionalisation. *Tellus A: Dynamic Meteorology and Oceanography*, 68(1), 28234.
1069
1070 Johnson, M., & Eicken, H. (2016). Estimating Arctic sea-ice freeze-up and break-up
1071 from the satellite record: A comparison of different approaches in the Chukchi and
1072 Beaufort Seas. *Elementa*, 4, 000124.
1073
1074 Kwok, R. (2007). Near zero replenishment of the Arctic multiyear sea ice cover at the
1075 end of 2005 summer. *Geophysical Research Letters*, 34(5).
1076
1077 Lebrun, M., Vancoppenolle, M., Madec, G., & Massonnet, F. (2019). Arctic sea-ice-free
1078 season projected to extend into autumn. *The Cryosphere*, 13(1), 79–96.
1079
1080 Lee, J.-Y., J. Marotzke, G. Bala, L. Cao, S. Corti, J.P. Dunne, F. Engelbrecht, E. Fischer, J.C.
1081 Fyfe, C. Jones, A. Maycock, J. Mutemi, O. Ndiaye, S. Panickal, and T. Zhou, 2021: Future
1082 Global Climate: Scenario-Based Projections and Near-Term Information. In *Climate*
1083 *Change 2021: The Physical Science Basis. Contribution of Working Group I to the Sixth*
1084 *Assessment Report of the Intergovernmental Panel on Climate Change*
1085 [Masson-Delmotte, V., P. Zhai, A. Pirani, S.L. Connors, C. Péan, S. Berger, N. Caud, Y.
1086 Chen, L. Goldfarb, M.I. Gomis, M. Huang, K. Leitzell, E. Lonnoy, J.B.R. Matthews, T.K.
1087 Maycock, T. Waterfield, O. Yelekçi, R. Yu, and B. Zhou (eds.)]. Cambridge University
1088 Press, Cambridge, United Kingdom and New York, NY, USA, pp. 553–672,

doi:10.1017/9781009157896.006.

Levine, X. J., Cvijanovic, I., Ortega, P., Donat, M. G., & Tourigny, E. (2021). Atmospheric feedback explains disparate climate response to regional Arctic sea-ice loss. *npj Climate and Atmospheric Science*, 4(1), 28.

Lukovich, J. V., & Barber, D. G. (2007). On the spatiotemporal behavior of sea ice concentration anomalies in the Northern Hemisphere. *Journal of Geophysical Research: Atmospheres*, 112(D13). <https://doi.org/10.1029/2006JD007836>

Markus, T., J. C. Stroeve, and J. Miller (2009), Recent changes in Arctic sea ice melt onset, freezeup, and melt season length, *J. Geophys. Res.*, 114, C12024, doi:10.1029/2009JC005436.

Maze, G., Mercier, H., Fablet, R., Tandeo, P., Radcenco, M. L., Lenca, P., ... & Le Goff, C. (2017). Coherent heat patterns revealed by unsupervised classification of Argo temperature profiles in the North Atlantic Ocean. *Progress in Oceanography*, 151, 275-292.

Meier, W. N., Stroeve, J., & Fetterer, F. (2007). Whither Arctic sea ice? A clear signal of decline regionally, seasonally and extending beyond the satellite record. *Annals of Glaciology*, 46, 428-434.

Mao, J., & Jain, A. K. (1996). A self-organizing network for hyperellipsoidal clustering (HEC). *Ieee transactions on neural networks*, 7(1), 16-29.

Maslanik, J., J. Stroeve, C. Fowler, and W. Emery (2011), Distribution and trends in Arctic sea ice age through spring 2011, *Geophys. Res. Lett.*, 38, L13502, doi:10.1029/2011GL047735.

Meier, W. N., F. Fetterer, A. K. Windnagel, and J. S. Stewart. (2021). NOAA/NSIDC Climate Data Record of Passive Microwave Sea Ice Concentration, Version 4 [Data Set]. Boulder, Colorado USA. National Snow and Ice Data Center. <https://doi.org/10.7265/efmz-2t65>. Date Accessed 15-07-2024.

Meier, W. N., Stewart, J. S., Windnagel, A., & Fetterer, F. M. (2022). Comparison of hemispheric and regional sea ice extent and area trends from NOAA and NASA passive microwave-derived climate records. *Remote Sensing*, 14(3), 619.

Meier, W. N., & Stroeve, J. (2022). An updated assessment of the changing Arctic sea ice cover. *Oceanography*, 35(3/4), 10-19.

Meier, Walter N., and J. Scott Stewart. (2023). NSIDC Land, Ocean, Coast, Ice, and Sea Ice Region Masks. NSIDC Special Report 25. Boulder CO, USA: National Snow and Ice Data Center. <https://nsidc.org/sites/default/files/documents/technical-reference/nsidc-special-report-25.pdf>

1136
 1137 Parkinson, C.L., J.C. Comiso, H.J. Zwally, D.J. Cavalieri, P. Gloersen, and W.J. Campbell,
 1138 (1987). Arctic sea ice, 1973-1976: Satellite passive-microwave observations, NASA
 1139 Special Publication, SP-489, 296 pp., <https://ntrs.nasa.gov/citations/19870015437>.
 1140
 1141 Parkinson, C.L., D.J. Cavalieri, P. Gloersen, H.J. Zwally, and J.C. Comiso, (1999). Arctic
 1142 sea ice extents, areas, and trends, 1978–1996, *J. Geophys. Res.*, 104(C9),
 1143 20837–20856, <https://doi.org/10.1029/1999JC900082>.
 1144
 1145 Parkinson, C. L., & Cavalieri, D. J. (2008). Arctic sea ice variability and trends,
 1146 1979–2006. *Journal of Geophysical Research: Oceans*, 113(C7).
 1147
 1148 Parkinson, C. L. (2014), Spatially mapped reductions in the length of the Arctic
 1149 sea ice season, *Geophys. Res. Lett.*, 41, 4316–4322, doi:10.1002/2014GL060434
 1150
 1151 Parkinson, C. L., and J. C. Comiso (2013), On the 2012 record low Arctic sea ice cover:
 1152 Combined impact of preconditioning and an August storm, *Geophys. Res. Lett.*, 40,
 1153 1356–1361, doi:10.1002/grl.50349
 1154
 1155 Parkinson, C.L.; Comiso, J.C.; Zwally, H.J.; Cavalieri, D.J.; Gloersen, P.; Campbell, W.J.
 1156 Arctic Sea Ice, 1973–1976: Satellite Passive-Microwave Observations; NASA SP-489;
 1157 National Aeronautics and Space Administration: Washington, DC, USA, 1987; p. 296.
 1158 Peng, G., & Meier, W. N. (2018). Temporal and regional variability of Arctic sea-ice
 1159 coverage from satellite data. *Annals of Glaciology*, 59(76pt2), 191-200.
 1160
 1161 Pedregosa, F., Michel, V., Grisel, O., Blondel, M., Prettenhofer, P., Weiss, R., et al. (2011).
 1162 Scikit-learn: Machine learning in Python
 1163
 1164 Peng, G., & Meier, W. N. (2018). Temporal and regional variability of Arctic sea-ice
 1165 coverage from satellite data. *Annals of Glaciology*, 59(76pt2), 191-200.
 1166
 1167
 1168 Pithan, F., & Mauritsen, T. (2014). Arctic amplification dominated by temperature
 1169 feedbacks in contemporary climate models. *Nature geoscience*, 7(3), 181-184.
 1170
 1171 Petty, A. A., Stroeve, J. C., Holland, P. R., Boisvert, L. N., Bliss, A. C., Kimura, N., & Meier,
 1172 W. N. (2018). The Arctic sea ice cover of 2016: a year of record-low highs and
 1173 higher-than-expected lows. *The Cryosphere*, 12(2), 433-452.
 1174
 1175 Przybylak, R. (2002). Variability of air temperature and atmospheric precipitation in
 1176 the Arctic. Dordrecht, etc., Kluwer Academic Publishers
 1177
 1178 Przybylak, R. (2007). Recent air-temperature changes in the Arctic. *Annals of Glaciology*,
 1179 46, 316-324.
 1180
 1181 Raphael, M. N., & Hobbs, W. (2014). The influence of the large-scale atmospheric
 1182 circulation on Antarctic sea ice during ice advance and retreat seasons:
 1183 RAPHAEL AND HOBBS; ANTARCTIC SEA ICE ADVANCE AND RETREAT.

1184 Geophysical Research Letters, 41(14), 5037–5045.
 1185 <https://doi.org/10.1002/2014GL060365>
 1186
 1187 Regan, H. C., Rampal, P., Ólason, E., Boutin, G., & Korosov, A. (2022). Modelling the
 1188 evolution of Arctic multiyear sea ice over 2000–2018. *The Cryosphere Discussions*,
 1189 2022, 1–28.
 1190
 1191 Ricker, R., Hendricks, S., Kaleschke, L., Tian-Kunze, X., King, J., and Haas, C. , (2017). A
 1192 weekly Arctic sea-ice thickness data record from merged CryoSat-2 and SMOS
 1193 satellite data, *The Cryosphere*, 11, 1607–1623,
 1194 <https://doi.org/10.5194/tc-11-1607-2017>.
 1195
 1196 Rolph, R. J., Feltham, D. L., & Schröder, D. (2020). Changes of the Arctic marginal ice
 1197 zone during the satellite era. *The Cryosphere*, 14(6), 1971–1984.
 1198
 1199 Rousseeuw, P. J. (1987). Silhouettes: a graphical aid to the interpretation and validation
 1200 of cluster analysis. *Journal of computational and applied mathematics*, 20, 53–65.
 1201
 1202 Shu, Q., Wang, Q., Årthun, M., Wang, S., Song, Z., Zhang, M., & Qiao, F. (2022). Arctic
 1203 Ocean Amplification in a warming climate in CMIP6 models. *Science advances*, 8(30),
 1204 eabn9755.
 1205
 1206 Siddon, E. C., Zador, S. G., & Hunt Jr, G. L. (2020). Ecological responses to climate
 1207 perturbations and minimal sea ice in the northern Bering Sea. *Deep Sea Research Part*
 1208 *II: Topical Studies in Oceanography*, 181, 104914.
 1209
 1210 Simon, A., Gastineau, G., Frankignoul, C., Rousset, C., and Codron, F. , (2021). Transient
 1211 climate response to Arctic sea-ice loss with two ice-constraining methods, *J. Climate*,
 1212 34, 3295–3310, <https://doi.org/10.1175/JCLI-D-20-0288.1>.
 1213
 1214 Smith, L. C., & Stephenson, S. R. (2013). New Trans-Arctic shipping routes navigable by
 1215 midcentury. *Proceedings of the National Academy of Sciences*, 110(13), E1191–E1195.
 1216
 1217 Smith, D. M., Eade, R., Andrews, M. B., Ayres, H., Clark, A., Chripko, S., and Walsh, A.
 1218 (2022) Robust but weak winter atmospheric circulation response to future Arctic
 1219 sea-ice loss, *Nat. Commun.*, 13, 1–15.
 1220
 1221 Song, L., Zhao, X., Wu, Y., Gong, J., & Li, B. (2025). Assessing Arctic marginal ice zone
 1222 dynamics from 1979 to 2023: insights into long-term variability and morphological
 1223 changes. *Environmental Research Letters*, 20(3), 034032.
 1224
 1225 Stammerjohn, S., Massom, R., Rind, D., and Martinson, D.: Regions of rapid sea ice
 1226 change (2012) An inter-hemispheric seasonal comparison, *Geophys. Res. Lett.*, 39,
 1227 L06501, <https://doi.org/10.1029/2012GL050874>.
 1228
 1229 Stock, C. A. et al. (2017). Reconciling fisheries catch and ocean productivity. *Proc. Natl*
 1230 *Acad. Sci. USA* 114, E1441–E1449.

1231 Stroeve, J. C., T. Markus, L. Boisvert, J. Miller, and A. Barrett (2014), Changes in Arctic
1232 melt season and implications for sea ice loss, *Geophys. Res. Lett.*, 41, 1216–1225,
1233 doi:10.1002/2013GL058951.

1234

1235 Stroeve, J. C., Crawford, A. D., and Stammerjohn, S. (2016). Using timing of ice retreat
1236 to predict timing of fall freeze-up in the Arctic, *Geophys. Res. Lett.*, 43, GL069314,
1237 <https://doi.org/10.1002/2016GL069314>.

1238

1239 Sutherland, P., & Dumont, D. (2018). Marginal ice zone thickness and extent due to
1240 wave radiation stress. *Journal of Physical Oceanography*, 48(8), 1885-1901.

1241

1242

1243 Valko, I. (2014). Differentiating Arctic provinces: a cluster analysis of geographic and
1244 geopolitical indicators. *Central European Journal of International & Security Studies*,
1245 8(4).

1246

1247 Vancoppenolle, M., L. Bopp, G. Madec, J. Dunne, T. Ilyina, P. R. Halloran, and N. Steiner
1248 (2013), Future Arctic Ocean primary productivity from CMIP5 simulations: Uncertain
1249 outcome, but consistent mechanisms, *Global Biogeochem. Cycles*, 27, 605–619,
1250 doi:10.1002/gbc.20055.

1251

1252 Wachter, P., Reiser, F., Friedl, P., & Jacobeit, J. (2021). A new approach to classification
1253 of 40 years of Antarctic sea ice concentration data. *International Journal of*
1254 *Climatology*, 41, E2683-E2699.

1255

1256

1257

1258

1259

1260

1261

1262

1263

1264

1265

1266

1267

1268

1269

1270

1271

1272

1273

1274

1275

1276

1277